
LATENT SPACE SMOOTHING FOR INDIVIDUALLY FAIR REPRESENTATIONS

PREPRINT

Momchil Peychev
 Department of Computer Science
 ETH Zurich, Switzerland
 momchil.peychev@inf.ethz.ch

Anian Ruoss*
 DeepMind
 London
 anianr@deepmind.com

Mislav Balunović, Maximilian Baader, Martin Vechev
 Department of Computer Science
 ETH Zurich, Switzerland
 {mislav.balunovic, mbaader, martin.vechev}@inf.ethz.ch

ABSTRACT

Fair representation learning transforms user data into a representation that ensures fairness and utility regardless of the downstream application. However, learning individually fair representations, i.e., guaranteeing that similar individuals are treated similarly, remains challenging in high-dimensional settings such as computer vision. In this work, we introduce LASSI, the first representation learning method for certifying individual fairness of high-dimensional data. Our key insight is to leverage recent advances in generative modeling to capture the set of similar individuals in the generative latent space. This enables us to learn individually fair representations that map similar individuals close together by using adversarial training to minimize the distance between their representations. Finally, we employ randomized smoothing to provably map similar individuals close together, in turn ensuring that local robustness verification of the downstream application results in end-to-end fairness certification. Our experimental evaluation on challenging real-world image data demonstrates that our method increases certified individual fairness by up to 90% without significantly affecting task utility.

Keywords fair representation learning, individual fairness, smoothing

1 Introduction

Deep learning models are increasingly deployed in critical domains, such as face detection [1], credit scoring [2], or crime risk assessment [3], where decisions of the model can have wide-ranging impacts on society. Unfortunately, the models and datasets employed in these settings are biased [4, 5], which raises concerns against their usage for such tasks and causes regulators to hold organizations accountable for the discriminatory effects of their models [6–10].

In this regard, fair representation learning [11] is a promising bias mitigation approach that transforms data to prevent discrimination regardless of the concrete downstream application while simultaneously maintaining high task utility. The approach is highly modular [12]: the *data regulator* defines the fairness notion, the *data producer* learns a fair representation that encodes the data, and the *data consumers* employ the transformed data in downstream tasks. Recent work successfully augmented fair representation learning with guarantees [13, 14], but its application to high-dimensional data, such as images, remains challenging.

Key challenge: scaling to high-dimensional data and real-world models The two central challenges of *individually* fair representation learning, which requires similar individuals to be treated similarly, are: (i) designing a suitable input similarity metric [11, 15] and (ii) enforcing that similar individuals are *provably* treated similarly according to

*Work partially done while the author was at ETH Zurich.

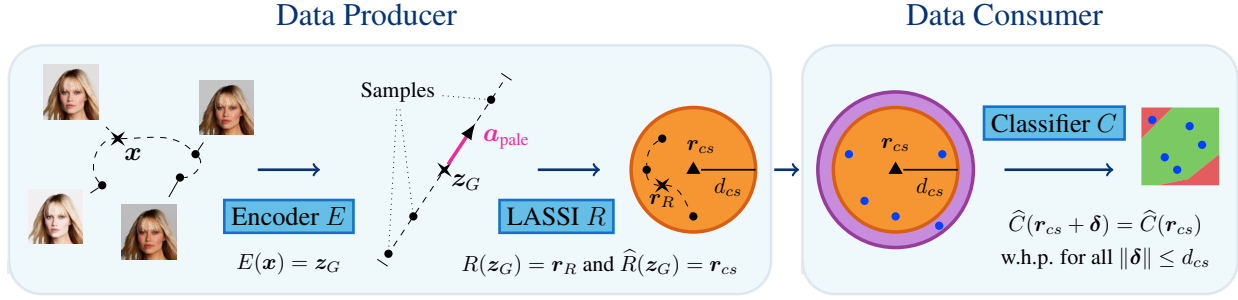


Figure 1: Overview of our framework LASSI. The left part shows the data producer who captures the set of individuals similar to x by interpolating along the attribute vector a_{pale} . The data producer then uses adversarial training and center smoothing to compute a representation that provably maps all similar points into the ℓ_2 -ball of radius d_{cs} around r_{cs} . The right part shows the data consumer who can certify individual fairness, i.e., prove that all similar individuals receive the same classification outcome, of the end-to-end model by checking whether the certified radius obtained via randomized smoothing exceeds d_{cs} .

that metric. For low-dimensional tabular data, prior work has typically measured input similarity in terms of the input features (age, income, etc.), using, e.g., logical constraints [14] or weighted ℓ_p -metrics [16]. However, characterizing the similarity of high-dimensional data, such as images, at the input-level, e.g., by comparing pixels, is infeasible. Moreover, proving that all points in the infinite set of similar individuals obtain the same classification requires propagating this set through the model. Unfortunately, for high-dimensional applications this is unattainable for prior work using (mixed-integer) linear programming solvers [17, 18], which only scale to small networks.

This work In this work, we introduce latent space smoothing for individually fair representations (LASSI), a method that addresses both of the above challenges. Our approach leverages two recent advances: the emergence of powerful generative models [19], which enable the definition of image similarity for individual fairness, and the scalable certification of deep models [20], which allows proving individual fairness. A high-level overview of our approach is shown in Fig. 1. Concretely, we use generative modeling [19] to enable data regulators to define input similarity by varying a continuous attribute of the image, such as pale skin in Fig. 1. To enforce that similar individuals are provably treated similarly, we further base our approach on smoothing: (i) the data producer uses center smoothing [21] to learn a representation that provably maps similar individuals close together, and (ii) the data consumer certifies local ℓ_2 -robustness using randomized smoothing [20], thereby proving individual fairness of the end-to-end model. Therefore, our approach enables data regulators to impose fairness notions of the form: *“For a given person, all people differing only in skin tone should receive the same classification”* and allows data producers and consumers to independently learn a representation and classification models that provably enforce this notion.

To measure input similarity, the data producer leverages the ability of a bijective generative model (with an encoder E) to interpolate along the direction of an attribute vector in the latent space, which is infeasible in the pixel space. As a result, the set of similar individuals can be defined by a line segment in the latent space (center part of the data producer in Fig. 1), corresponding to an elaborate curve in the input space (left part of the data producer in Fig. 1), which cannot be concisely captured by, e.g., an ℓ_p -ball. Thus, the data producer learns a representation R that maps all points of the latent line segment close together in the representation space by using adversarial training to minimize the distance between similar individuals. However, as adversarial training cannot provide guarantees on this maximum distance, the data producer uses center smoothing [21] to adjust the representation such that its *smoothed* version \hat{R} provably maps all similar points into an ℓ_2 -ball of radius d_{cs} around a center r_{cs} with high probability (right part of the data producer in Fig. 1). Finally, the data consumer only needs to prove that the certified radius (violet in the data consumer part of Fig. 1) of its *smoothed* classifier \hat{C} around r_{cs} is larger than d_{cs} to obtain an individual fairness certificate for the end-to-end model $M := \hat{C} \circ \hat{R} \circ E$.

Our experimental evaluation on several image classification tasks shows that training with LASSI significantly increases the number of individuals for which we can certify individual fairness, with respect to multiple different sensitive attributes, as well as their combinations. Overall, we certify up to 90% more than the baselines. Furthermore, we demonstrate that the representations obtained by LASSI can be used to solve classification tasks that were unseen during training. We also use a procedurally generated dataset to confirm that the certificates obtained with the generative model are sound and transfer to the ground truth dataset.

Main contributions We make the following contributions:

- A novel input similarity metric for high-dimensional data defined via interpolation in the latent space of generative models.
- A scalable representation learning method with individual fairness certification for models using high-dimensional data via randomized smoothing.
- A large-scale evaluation of our method on various image classification tasks.

2 Related Work

In this work, we consider individual fairness, which requires that similar individuals be treated similarly [22]. In contrast, group fairness enforces specific classification statistics to be equal across different groups of the population [22, 23]. While both fairness notions are desirable, they also both suffer from certain shortcomings. For instance, models satisfying group fairness may still discriminate against individuals [22] or subgroups [24]. In contrast, the central challenge limiting practical adoption of individual fairness is the lack of a widely accepted similarity metric [15]. While recent work has made progress in developing similarity metrics for tabular data [25–29], defining similarity concisely for high-dimensional data remains challenging and is a key contribution of our work.

Fair representation learning A wide range of methods has been proposed to learn fair representations of user data. Most of these works consider group fairness and employ techniques such as adversarial learning [30–33], disentanglement [34–36], duality [37], low-rank matrix factorization [38], and distribution alignment [39–41]. Fair representation learning for individual fairness has recently gained attention, with similarity metrics based on logical formulas [14], Wasserstein distance [42, 43], fairness graphs [44], and weighted ℓ_p -norms [11]. Unfortunately, none of these approaches can capture the similarity between individuals for the high-dimensional data we consider in our work.

Bias in high-dimensional data A long line of work has investigated the biases of models operating on high-dimensional data, such as images [45, 46] and text [47–50], showing, e.g., that black women obtain lower accuracy in commercial face classification [4, 5, 51]. Importantly, these models not only learn but also amplify the biases of the training data [52, 53], even for balanced datasets [54]. A key challenge for bias mitigation in high-dimensional settings is that, unlike tabular data, sensitive attributes such as age or skin tone are not directly encoded as features. Thus, prior work has often relied on generative models [55–62] or computer simulations [63] to manipulate these sensitive attributes and check whether the perturbed instances are classified the same. However, unlike our work, these methods only tested for bias empirically and thus do not provide fairness guarantees. Recent work also explored using generative models to define [64, 65] or certify [66] robustness, but without focusing on fairness.

Fairness certification Regulatory agencies are increasingly holding organizations accountable for the discriminatory effects of their machine learning models [6–10]. Accordingly, designing algorithms with fairness guarantees has become an active area of research [13, 39, 67–70]. However, unlike our work, most approaches for individual fairness certification consider pretrained models and thus cannot be employed in fair representation learning [16, 71, 72]. In contrast, Ruoss et al. [14] learn individually fair representations with provable guarantees for low-dimensional tabular data, providing a basis for our approach. However, neither the similarity notions nor the certification methods employed by [14] scale to high-dimensional data, which is the primary focus of our work.

3 Background

This section provides the necessary background on individual fairness, fair representation learning, generative modeling, and randomized smoothing.

Individual fairness The seminal work of Dwork et al. [22] defined individual fairness as “treating similar individuals similarly”. In this work, we consider the concrete instantiation of this notion from [14], which states that a model $M : \mathbb{R}^n \mapsto \mathcal{Y}$ is individually fair for a point $\mathbf{x} \in \mathbb{R}^n$ (e.g., an image of a person) if all individuals similar to \mathbf{x} , as measured by a binary input similarity metric $\phi : \mathbb{R}^n \times \mathbb{R}^n \mapsto \{0, 1\}$, are classified the same by M , i.e.,

$$\forall \mathbf{x}' \in \mathbb{R}^n : \phi(\mathbf{x}, \mathbf{x}') \implies M(\mathbf{x}) = M(\mathbf{x}'). \quad (1)$$

For example, a credit rating algorithm is individually fair for a given person if all similar applicants (e.g., similar income and repayment history) receive the same credit rating. Our goal is to learn a model M that maximizes the number of points \mathbf{x} from the distribution for which we can *guarantee* that Eq. (1) is satisfied. Defining a suitable input similarity metric ϕ is one of the key challenges limiting practical applications of individual fairness, and in Sec. 4.1 we will show how to employ generative modeling to overcome this obstacle for high-dimensional data.

Fair representation learning Fair representation learning [11] partitions the model $M : \mathbb{R}^n \mapsto \mathcal{Y}$ into a data producer $P : \mathbb{R}^n \mapsto \mathbb{R}^k$, which maps input points $\mathbf{x} \in \mathbb{R}^n$ into a representation space \mathbb{R}^k that satisfies a given fairness notion while maintaining downstream utility, and a data consumer $C : \mathbb{R}^k \mapsto \mathcal{Y}$ that solves a downstream task taking

only the transformed data points $\mathbf{r} := P(\mathbf{x}) \in \mathbb{R}^k$ as inputs. Importantly, the consumers (potentially indifferent to fairness) can employ standard training methods to obtain fair classifiers that are useful across a variety of different tasks. We base our approach on the LCIFR framework [14], which learns representations with individual fairness guarantees for low-dimensional tabular data. LCIFR defines a family of similarity notions and leverages (mixed-integer) linear programming methods for fairness certification. However, high-dimensional applications are out of reach for LCIFR because both the similarity notions and linear programming methods are tailored to low-dimensional tabular data. In particular, similarity is defined via logical formulas operating on the features of \mathbf{x} , which is infeasible for, e.g., images, which cannot be compared solely at the pixel level. Moreover, while linear programming methods work well for small networks, they do not scale to real-world computer vision models. In this work, we show how to resolve these two key concerns to generalize the high-level idea of LCIFR to real-world, high-dimensional applications.

Generative modeling Normalizing flows, such as Glow [19], recently emerged as a promising generative modeling approach due to their exact log-likelihood evaluation, efficient inference and synthesis, and useful latent space for downstream tasks. Unlike GANs [73] or VAEs [74], normalizing flows are bijective models consisting of an encoder $E : \mathbb{R}^n \rightarrow \mathbb{R}^q$ and a decoder $D : \mathbb{R}^q \rightarrow \mathbb{R}^n$ for which $\mathbf{x} = D(E(\mathbf{x}))$. For Glow the input space \mathbb{R}^n and the latent space \mathbb{R}^q have the same dimensionality, i.e., $n = q$. Glow’s latent space captures important data attributes, thus enabling latent space interpolation such as changing the age of a person in an image. While attribute manipulation via latent space interpolation has also been investigated in the fairness context for GANs and VAEs [55, 57–59, 61], Glow’s key advantage is the existence of an encoder (unlike GANs, which cannot represent an input point in the latent space efficiently) and the bijectivity of the end-to-end model (VAEs cannot reconstruct the input point exactly). Our key idea is to leverage Glow to define image similarity by interpolating along the directions defined by certain sensitive attributes in the latent space.

Randomized Smoothing Unlike (mixed-integer) linear programming [17, 18], randomized smoothing approaches [20] can compute local robustness guarantees for any type of classifier $C : \mathbb{R}^k \mapsto \mathcal{Y}$, regardless of its complexity and scale. To that end, Cohen et al. [20] construct a smoothed classifier $\hat{C} : \mathbb{R}^k \mapsto \mathcal{Y}$, which returns the most probable classification of C for an input $\mathbf{r} \in \mathbb{R}^k$ when perturbed by random noise from $\mathcal{N}(0, \sigma_{rs}^2 I)$. Using a sampling-based approach, [20] establish a local robustness guarantee of the form: $\forall \delta \in \mathbb{R}^k$ such that $\|\delta\|_2 < d_{rs}$ we have $\hat{C}(\mathbf{r} + \delta) = \hat{C}(\mathbf{r})$ with probability $1 - \alpha_{rs}$, where α_{rs} can be made arbitrarily small. Thus, \hat{C} will classify all points in the ℓ_2 -ball of radius d_{rs} around \mathbf{r} the same with high probability. Recently, Kumar and Goldstein [21] introduced center smoothing, which extends this approach from classification to multidimensional regression. Concretely, for a function $R : \mathbb{R}^q \mapsto \mathbb{R}^k$, center smoothing uses sampling and approximation to compute a smooth version $\hat{R} : \mathbb{R}^q \mapsto \mathbb{R}^k$, which maps $\mathbf{z} \in \mathbb{R}^q$ to the center point $\mathbf{r}_{cs} := \hat{R}(\mathbf{z})$ of a minimum enclosing ball containing at least half of the points $\mathbf{r}_i \sim R(\mathbf{z} + \mathcal{N}(0, \sigma_{cs}^2 I))$ for $i \in \{1, \dots, m\}$. Then, for $\epsilon > 0$ and $\forall \mathbf{z}' \in \mathbb{R}^q$ such that $\|\mathbf{z} - \mathbf{z}'\|_2 \leq \epsilon$, we have $\|\hat{R}(\mathbf{z}) - \hat{R}(\mathbf{z}')\|_2 \leq d_{cs}$ with probability at least $1 - \alpha_{cs}$. That is, center smoothing computes a sound upper bound d_{cs} on the ℓ_2 -ball of the function outputs of \hat{R} for all points in the ℓ_2 -ball of radius ϵ around \mathbf{z} .

4 High-Dimensional Individually Fair Representations

In this section, we describe how our method defines a set of similar individuals (Sec. 4.1), learns individually fair representations for these points (Sec. 4.2), and finally, certifies individual fairness for them (Sec. 4.4). Our approach is general, but we focus on images for presentational purposes.

4.1 Similarity via a Generative Model

We consider two individuals \mathbf{x} and \mathbf{x}' to be similar if they differ only in their continuous sensitive attributes. However, semantic attributes, such as skin color, cannot be captured conveniently via the input features of \mathbf{x} . Thus, our key idea is to define similarity in the latent space of a generative model G . We compute a vector $\mathbf{a} \in \mathbb{R}^q$ associated with the sensitive attribute, such that interpolating along the direction of \mathbf{a} in the latent space and reconstructing back to the input space results in a meaningful semantic transformation of that attribute. There is active research investigating different ways of computing \mathbf{a} [57, 75], and we will empirically show that our method is compatible with any such method.

Computing \mathbf{a} We define individual similarity in the latent space of Glow [19]. Our method is orthogonal to the actual computation of \mathbf{a} , which we demonstrate by instantiating two different attribute vector types. Let $\mathbf{z}_G = E(\mathbf{x})$ be the latent code of \mathbf{x} in the generative latent space. First, following [19], we compute \mathbf{a} by calculating the average latent vectors $\mathbf{z}_{G, pos}$ for samples with the attribute and $\mathbf{z}_{G, neg}$ for samples without it and setting \mathbf{a} to their difference, i.e., $\mathbf{a} = \mathbf{z}_{G, pos} - \mathbf{z}_{G, neg}$. Second, following [57], we train a linear classifier $\text{sign}(\mathbf{a}^\top \mathbf{z}_G + b)$ to predict the presence of the attribute from \mathbf{z}_G and take \mathbf{a} to be the vector orthogonal to the decision boundary of the linear classifier. In this case, we normalize \mathbf{a} to have unit ℓ_2 norm. In both cases, moving in one direction of \mathbf{a} in the latent space increases the presence of the attribute and interpolating in the opposite direction decreases it.

Individual similarity in latent space Using the generative model G and the attribute vector \mathbf{a} , we define the set of individuals similar to \mathbf{x} in the latent space of G as $S(\mathbf{x}) := \{\mathbf{z}_G + t \cdot \mathbf{a} \mid |t| \leq \epsilon\} \subseteq \mathbb{R}^q$ (see bottom of Fig. 2). Here, ϵ denotes the maximum perturbation level that we can apply to the attribute. We consider G , \mathbf{a} , and ϵ to be a part of the similarity specification set by the data regulator. Crucially, $S(\mathbf{x})$ contains an infinite number of points but is compactly represented in the latent space of G as a line segment. In contrast, the same set represented directly in the input space, $S_i(\mathbf{x}) := \{D(\mathbf{z}) \mid \mathbf{z} \in S(\mathbf{x})\} \subseteq \mathbb{R}^n$, obtained by decoding the latent representations in $S(\mathbf{x})$ with the decoder D , cannot be abstracted conveniently (top of Fig. 2). Moreover, this approach for constructing $S(\mathbf{x})$ can be extended to multiple sensitive attributes by interpolating along their attribute vectors simultaneously. Referring back to the notation in Sec. 3, we formally define the input similarity metric ϕ so that $\phi(\mathbf{x}, \mathbf{x}') \iff \mathbf{x}' \in S_i(\mathbf{x})$.

4.2 Learning Individually Fair Representations

Assuming that the generative model $G = D \circ E$ is pretrained and given (e.g., by the data regulator), in this section we describe the learning of the representation $R : \mathbb{R}^q \mapsto \mathbb{R}^k$, which maps from the generative latent space \mathbb{R}^q directly to the representation space \mathbb{R}^k . The representation R is trained separately from the data consumer, the classifier C , whose training is explained in the next section.

Adversarial loss We encourage similar treatment for all points in $S_i(\mathbf{x})$ by training R to map them close to each other in \mathbb{R}^k . This can be achieved by minimizing the loss

$$\mathcal{L}_{adv}(\mathbf{x}) = \max_{\mathbf{z}' \in S(\mathbf{x})} \|R(\mathbf{z}_G) - R(\mathbf{z}')\|_2. \quad (2)$$

Minimizing $\mathcal{L}_{adv}(\mathbf{x})$ is a min-max optimization problem, and adversarial training [76] is known to work well in such settings. Because the underlying domain of the inner maximization problem is simply the line segment $S(\mathbf{x})$, we perform a random adversarial attack in which we sample s points $\mathbf{z}_i \sim \mathcal{U}(S(\mathbf{x}))$ uniformly at random from $S(\mathbf{x})$ and approximate $\mathcal{L}_{adv}(\mathbf{x}) \approx \max_{i=1}^s \|R(\mathbf{z}_G) - R(\mathbf{z}_i)\|_2$. This efficient attack is typically more effective [77] than the first-order methods such as FGSM [78] and PGD [76] when the search space is low-dimensional.

Classification loss To ensure that the learned representations remain useful for downstream tasks, we introduce an auxiliary classifier C_{aux} to predict a ground truth target label y by adding an additional classification loss term:

$$\mathcal{L}_{cls}(\mathbf{x}, y) = \text{cross_entropy}((C_{aux} \circ R)(\mathbf{z}_G), y). \quad (3)$$

Reconstruction loss The downstream task may not always be known to the data producer a priori, and thus our representations should ideally transfer to a variety of such tasks. To that end, we optionally utilize a reconstruction loss, which is designed to preserve the signal from the original data [14, 33]:

$$\mathcal{L}_{recon}(\mathbf{x}) = \|\mathbf{z}_G - Q(R(\mathbf{z}_G))\|_2, \quad (4)$$

where $Q : \mathbb{R}^k \mapsto \mathbb{R}^q$ denotes a reconstruction network.

The representation R , the auxiliary classifier C_{aux} , and the reconstruction network Q are trained jointly using stochastic gradient descent to minimize the combined objective

$$\lambda_1 \mathcal{L}_{cls}(\mathbf{x}, y) + \lambda_2 \mathcal{L}_{adv}(\mathbf{x}) + \lambda_3 \mathcal{L}_{recon}(\mathbf{x}). \quad (5)$$

Trading off fairness, accuracy, and transferability is a multi-objective optimization problem, an active area of research. Here, we follow [14, 33] and use a linear scalarization scheme, with the hyperparameters λ_1 , λ_2 and λ_3 balancing the three losses, but our method is also compatible with other schemes [79–81].

4.3 Training the Classifier C

Once we have learned the representation R , we can use it to train any classifier C (often different from the auxiliary one C_{aux}). As we will apply smoothing to C , we train it by adding isotropic Gaussian noise to its inputs during the training process, as in [20]. We use the outputs of $R \circ E$ (and not the smoothed version $\widehat{R} \circ E$) as inputs to train C , since repeatedly smoothing the pipeline at this step is computationally expensive and because the distance between the smoothed and the unsmoothed outputs is generally small [21].

4.4 Certifying Individual Fairness via Latent Space Smoothing

With R and C trained as described above, we now construct the end-to-end model $M : \mathbb{R}^n \mapsto \mathcal{Y}$ for which, given an input \mathbf{x} , we can certify individual fairness of the form

$$\forall \mathbf{x}' \in S_i(\mathbf{x}) : M(\mathbf{x}) = M(\mathbf{x}'). \quad (6)$$

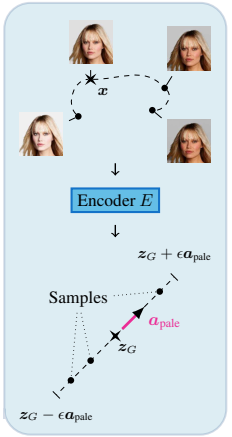


Figure 2: Similarity in the latent space.

Algorithm 1 Certifying the individual fairness of $\widehat{C} \circ \widehat{R} \circ E$ for the input \mathbf{x} .

```

function CERTIFY( $E, R, C, \mathbf{x}$ )
   $r_{cs} = \widehat{R}(\mathbf{z}_G)$  and  $d_{cs}$  from center smoothing [21], where  $\mathbf{z}_G = E(\mathbf{x})$ .
  if center smoothing abstained then return ABSTAIN
  Smooth  $C$  [20] to obtain the certified radius  $d_{rs}$  around  $r_{cs}$  (i.e., same classification).
  if  $d_{cs} < d_{rs}$  then return CERTIFIED
  else return NOT CERTIFIED

```

Given a point \mathbf{z} in the latent space of G , we define the function $g_{\mathbf{z}}(t) := R(\mathbf{z} + t \cdot \mathbf{a})$ for $t \in \mathbb{R}$. We apply the center smoothing procedure presented by [21] to obtain $\widehat{g}_{\mathbf{z}}$, the smoothed version of $g_{\mathbf{z}}$, and define $\widehat{R}(\mathbf{z}) := \widehat{g}_{\mathbf{z}}(0)$ such that for all $\mathbf{z}' \in S(\mathbf{x})$, $\|\widehat{R}(\mathbf{z}) - \widehat{R}(\mathbf{z}')\|_2 \leq d_{cs}$ (see Fig. 3). Moreover, we smooth the classifier C to obtain its ℓ_2 -robustness radius d_{rs} . If $d_{cs} < d_{rs}$, then the end-to-end model $M = \widehat{C} \circ \widehat{R} \circ E$ certifiably satisfies individual fairness at \mathbf{x} (as defined in Eq. (6)) with high probability. Concretely, if we instantiate center smoothing with confidence α_{cs} and randomized smoothing with confidence α_{rs} , the individual fairness certificate holds with probability at least $1 - \alpha_{cs} - \alpha_{rs}$ (union bound). The compositional certification procedure is summarized in Alg. 1 and its correctness is formalized in Thm. 4.1 (with a detailed proof in App. A).

Theorem 4.1. *Assume that we have a bijective generative model $G = D \circ E$ used to define the similarity set $S_i(\mathbf{x})$ for a given input \mathbf{x} . Let Alg. 1 perform center smoothing [21] with confidence $1 - \alpha_{cs}$ and randomized smoothing [20] with confidence $1 - \alpha_{rs}$. If Alg. 1 returns CERTIFIED for the input \mathbf{x} , then the end-to-end model $M = \widehat{C} \circ \widehat{R} \circ E$ is individually fair for \mathbf{x} with respect to $S_i(\mathbf{x})$ with probability at least $1 - \alpha_{cs} - \alpha_{rs}$.*

5 Experiments

We now present our experimental evaluation of LASSI. Our key findings are that: (i) LASSI reliably enforces individual fairness and keeps accuracy high, (ii) LASSI is applicable to a wide range of sensitive attributes and attribute vectors, (iii) the representations learned with LASSI can transfer to unseen tasks, and (iv) guarantees of LASSI obtained using generative models are sound with respect to known ground-truth labels of similar individuals.

Datasets We evaluate LASSI on three datasets. CelebA [82] contains 202,599 aligned and cropped face images of real-world celebrities. The images are annotated with the presence or absence of 40 face attributes with various correlations between them [57]. As CelebA is highly imbalanced, we also experiment with FairFace [83], which is balanced on race and contains 97,698 released images (padding 0.25) of individuals from 7 race and 9 age groups. We split the training set randomly (80:20 ratio) and evaluate on the validation set because the test set is not publicly shared. Finally, the 3D Shapes dataset [84] consists of images of 3D shapes that are procedurally generated from 6 independent latent factors: floor hue, wall hue, object hue, scale, and orientation. The 3D Shapes dataset is typically used to investigate disentanglement properties of unsupervised learning methods (e.g., in the context of fairness [35]). We provide further information about the datasets (including experimental “unfairness” of different sensitive attributes computed on CelebA) in App. B.

Experimental setup The following setup is used for all experiments, unless stated otherwise. We use images of size 64×64 , and for each dataset pretrain a Glow model G with 4 blocks of 32 flows, using an open-source PyTorch [85] implementation [86]. We use $\mathbf{a} = \mathbf{z}_{G, \text{pos}} - \mathbf{z}_{G, \text{neg}}$ and set $\epsilon = 1$ such that $S_i(\mathbf{x})$ contains realistic high-quality reconstructions. Thus, the similarity specification (Sec. 4.1) for enforcing individual fairness is determined by the generative model G and the radius ϵ . We implement the representation R as a fully-connected network that propagates Glow’s latent code of an input \mathbf{x} through two hidden layers of sizes 2048 and 1024 (with ReLU activations), mapping to a 512-dimensional space. The final layer applies zero mean and unit variance normalization ensuring that all components of the output of R are in the same range when Gaussian noise is added during smoothing. A linear classifier C is used for predicting the target label.

Our fairness-unaware baseline (denoted as Naive) is standard representation learning of R without adversarial and reconstruction losses ($\lambda_2 = \lambda_3 = 0$). When training LASSI, we set the classification loss weight $\lambda_1 = 1$, except for the transfer learning experiments. A recent work [61] proposed generating synthetic images with a GAN [73] to balance the dataset. Their method is not concerned with individual fairness and their transformation of latent representations may change other, non-sensitive attributes. Nevertheless, we compare with a similar data augmentation strategy (denoted as DataAug) randomly sampling s additional images from $S_i(\mathbf{x})$ for each training sample. We do

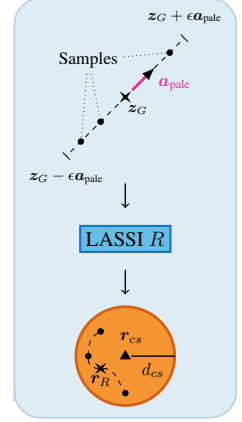


Figure 3: Center smoothing the similarity set.

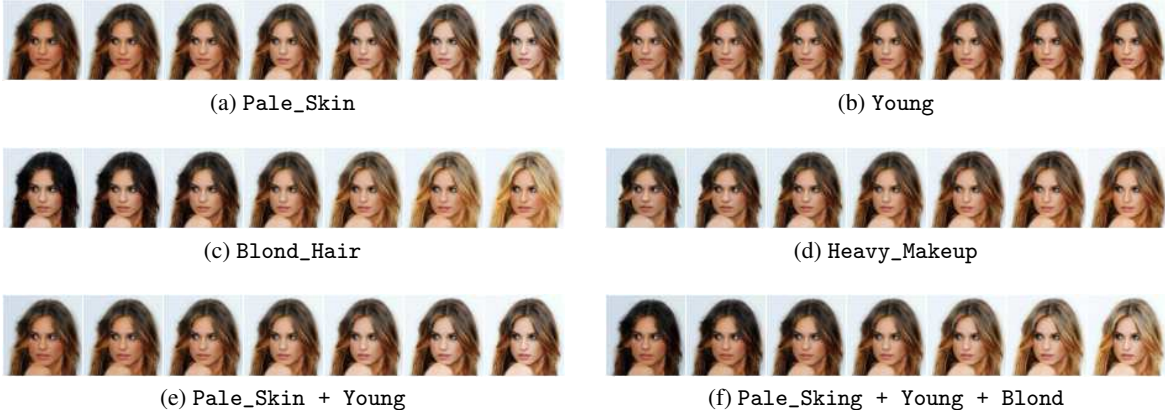


Figure 4: Similar points from $S_i(\mathbf{x})$, as reconstructed by Glow, for multiple combinations of sensitive attributes. Central images correspond to the original input. We vary t uniformly (left to right) in the $[-\frac{\epsilon}{\sqrt{n}}, \frac{\epsilon}{\sqrt{n}}]$ range, $n =$ number of sensitive attributes, $\epsilon = 1$. For $n > 1$, all attribute vectors are multiplied by the same t .

Table 1: Evaluation of LASSI on the CelebA dataset, showing that LASSI significantly increases certified individual fairness compared to the baselines without affecting the classification accuracy, even increasing it for imbalanced tasks. Reported means averaged over 5 runs, see App. D for standard deviations.

Task	Sensitive attribute(s)	Naive		DataAug [61]		LASSI (ours)	
		Acc	Fair	Acc	Fair	Acc	Fair
Smiling	Pale_Skin	86.3	0.6	85.7	12.2	85.9	98.0
	Young	86.3	38.2	85.9	43.0	86.4	98.9
	Blond_Hair	86.4	3.4	86.6	9.4	86.4	94.7
	Heavy_Makeup	86.4	0.4	85.3	13.7	85.6	91.4
	Pale+Young	86.0	0.4	85.8	9.9	85.8	97.3
	Pale+Young+Blond	86.2	0.0	86.4	3.6	85.5	86.5
Earrings	Pale_Skin	81.4	24.3	81.0	40.5	85.0	98.5
	Young	81.4	59.2	79.9	72.0	84.5	98.0
	Blond_Hair	81.4	9.2	82.2	30.5	84.8	96.2
	Heavy_Makeup	81.6	20.5	80.3	49.2	82.3	98.7

not compare with LCIFR [14] as our individual similarity specifications cannot be directly encoded as logical formulas over the input features of \mathbf{x} and because its certification is based on expensive solvers that do not scale to Glow and large models.

We list all selected hyperparameters for all experiments, based on an extensive hyperparameter search on the validation sets, in App. C (details provided for the CelebA dataset). The hyperparameter study shows that LASSI works for a wide range of hyperparameter values and demonstrates that λ_2 controls the trade-off between accuracy and fairness. We report the accuracy and the certified individual fairness of the models measured on 312 samples from CelebA’s test set (every 64-th), 343 samples from FairFace’s test set (every 32-nd) and 300 samples from 3D Shapes’s test set (every 320-th). The certified fairness refers to the number of samples for which Alg. 1 returns CERTIFIED, i.e., for which we can prove that Eq. (6) holds, guaranteeing that all similar individuals (according to our similarity definition) are classified the same. The evaluation of a single sample takes up to 6 seconds due to the sampling required by the smoothing procedures, which is why we do not report results on the whole test sets. We ran the experiments on GeForce RTX 2080 Ti GPUs and will release all the code and models to reproduce our results.

Single sensitive attribute We experiment with 4 different continuous sensitive attributes from CelebA: Pale_Skin, Young, Blond_Hair and Heavy_Makeup on two tasks: predicting Smiling and Earrings. We chose attributes with different balance ratios that have also been used in prior work [57], while avoiding attributes that perpetuate harmful stereotypes [57] (e.g., avoiding Male). Glow can also be used to generate discrete attributes, but then fairness

Table 2: Evaluation with \mathbf{a} perpendicular to the linear decision boundary of the sensitive attribute [57] (Sec. 4.1) on the Smiling task, showing that LASSI is not limited to a specific attribute vector type.

Sensitive attribute(s)	Naive		DataAug [61]		LASSI (ours)	
	Acc	Fair	Acc	Fair	Acc	Fair
Pale_Skin	86.4	34.0	85.9	90.3	86.5	98.8
Young	86.3	73.1	86.2	90.3	86.8	97.9
Blond_Hair	86.2	71.4	86.1	88.8	86.7	98.8
Heavy_Makeup	86.2	11.5	86.3	87.4	86.8	98.8
Pale+Young	86.2	28.6	85.8	84.7	86.5	98.6
Pale+Young+Blond	86.2	23.7	85.9	82.2	86.4	98.7

Table 3: Transfer learning results, demonstrating that LASSI can still achieve high certified individual fairness even when the downstream tasks are not known.

Sens. attrib.:	Pale (P)		Young (Y)		Blond (B)		P+Y		P+Y+B	
	Acc	Fair	Acc	Fair	Acc	Fair	Acc	Fair	Acc	Fair
Smiling	86.2	93.1	86.0	95.5	85.1	93.8	85.9	92.2	85.1	87.1
High_Cheeks	81.7	92.6	82.3	96.0	81.4	92.2	80.8	93.0	80.6	84.5
Mouth_Open	81.5	91.2	82.4	94.3	82.4	87.5	81.6	90.1	82.5	80.8
Lipstick	88.3	94.0	85.8	95.8	86.8	91.2	85.1	90.6	86.2	81.0
Heavy_Makeup	86.5	93.0	83.5	95.3	85.6	89.3	83.7	90.0	83.3	80.5
Wavy_Hair	79.2	93.3	77.5	95.8	78.0	91.3	77.6	91.5	78.9	85.3
Eyebrows	78.3	92.1	78.3	94.7	78.9	89.6	77.8	92.2	78.7	85.6

certification can be done via enumeration because partial eyeglasses or hats, for example, are not plausible. Example images from $S_i(\mathbf{x})$ for a single \mathbf{x} are provided in Fig. 4. The Earrings task is considerably more imbalanced than Smiling, with the majority class obtaining 78.21% accuracy on our test subset.

We show the results in Tab. 1 averaged over 5 runs with different random seeds. The results indicate that data augmentation helps, but is not enough. LASSI significantly improves the certified fairness, compared to the baselines, with a minor loss of accuracy on Smiling and even acts as a helpful regularizer on the imbalanced Earrings task. In App. D we report the standard deviations demonstrating that LASSI consistently enforces individual fairness with low variance and further evaluate empirical (i.e., non-certifiable) fairness metrics.

Multiple sensitive attributes In the next experiment, we combine the sensitive attributes Pale_Skin, Young and Blond_Hair and predict Smiling. The similarity sets w.r.t. which we certify individual fairness are defined as $S(\mathbf{x}) = \{E(\mathbf{x}) + \sum_i t_i \cdot \mathbf{a}_i \mid \|\mathbf{t}\|_2 \leq \epsilon\}$. The results in Tab. 1 (rows 5 – 6) show that the certified fairness drops as the similarity sets become more complex, as expected, but LASSI still successfully enforces individual fairness in these cases.

Larger images and different attribute vectors Next, we explore if LASSI can also work with larger images. We increase the dimensionality of the CelebA images to 128×128, pretrain Glow with 5 blocks and keep the rest of the hyperparameters the same. The results are consistent with those already presented in Tab. 1: LASSI increases the certified individual fairness by up to 77% on the Smiling task. We also instantiate LASSI with the alternative attribute vector type introduced in Sec. 4.1 (with $\epsilon = 10$). Although interpolating along the vector which is perpendicular to the linear decision boundary of the sensitive attribute possibly reduces the correlations leaked into the similarity sets, Tab. 2 shows that LASSI still improves the certified fairness by up to 16% compared to the baselines, demonstrating that it can be useful for various attribute vector types. We provide further details of these experiments in App. D.

Transfer learning To demonstrate the modularity of our approach, we show that LASSI can learn fair and transferable representations which are useful for unseen downstream tasks. To that end, we turn off the classification loss, consistent with prior work [33] ($\lambda_1 = 0$, i.e., the representation R is trained unsupervised) and enable the reconstruction loss ($\lambda_3 = 0.1$). The reconstruction network Q has an architecture symmetric to that of R . In Tab. 3 we report the accuracies and the certified fairness on 7 different, relatively well-balanced, downstream tasks. The models perform slightly worse compared to the case where the downstream task is known in advance, but the obtained certified individual fairness is still consistently high – more than 80% for the most complex similarity specification (P+Y+B) and above 90% for the simpler ones. Standard deviations and baseline accuracies on these tasks are reported in App. D.

Table 4: Results on FairFace, demonstrating that LASSI can significantly improve the certified individual fairness even on balanced datasets. The adversarial loss weight is $\lambda_2 = 0.1$ for all models except Naive, the transfer models are trained on Age-2 with reconstruction loss weight $\lambda_3 = 0.1$, while LASSI is trained on the corresponding tasks ($\lambda_1 = 1$, $\lambda_3 = 0$).

Task	Naive		Transfer $_{\lambda_1=0}$		Transfer $_{\lambda_1=0.001}$		Transfer $_{\lambda_1=0.01}$		LASSI	
	Acc	Fair	Acc	Fair	Acc	Fair	Acc	Fair	Acc	Fair
Age-2	69.0	5.7	66.4	91.7	68.8	90.2	74.9	91.7	72.0	95.0
Age-3	67.0	0.0	63.0	85.6	63.7	86.5	67.7	88.1	65.1	90.9
Age (all)	42.2	0.0	34.3	72.0	35.0	73.8	37.1	77.5	41.5	66.0

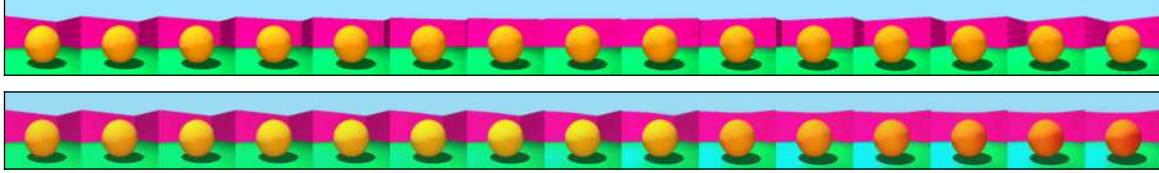


Figure 5: A sample shape at 15 different ground truth orientations (top) and the corresponding reconstructions obtained from interpolating along one of the generative model’s attribute vectors, $a_{1,15}$ (bottom), showing that the generative model reconstructions are close to the ground truth.

Training on FairFace dataset To verify that LASSI works well in different settings, we also evaluate on the FairFace [83] dataset. We select Race=Black as a sensitive attribute and predict Age. This is a very challenging multi-class task with around 60% state of the art accuracy. Therefore, we create two easier tasks: Age-2, predicting if an individual is younger or older than 30, and Age-3 with three target ranges: [0 – 19], [20 – 39], and 40+. Tab. 4 reports the results for $\epsilon = 0.5$ and $\sigma_{cs} = 0.325$. We verify that transfer learning also works in this setup by training on Age-2 and then transferring the representations to all three tasks. As the tasks are related, increasing the classification loss weight $\lambda_1 \in \{0, 0.001, 0.01\}$ on the base task, increases both the transfer downstream accuracy and the certified fairness. The highest certified fairness is generally obtained when the downstream task is known and the model is trained on it (LASSI, $\lambda_1 = 1$).

Certification with ground truth data An essential part of the evaluation is demonstrating that the fairness certificates obtained using the generative model transfer to ground truth data. Since CelebA does not contain images of the same individual with different attributes, e.g., the same individual with different skin colors, we use the 3D Shapes dataset [84], which provides images of the same object with varying latent factors. The goal is to show that the similarity set computed by Glow captures a given latent factor (as in Fig. 5), and thus certification with respect to this set will result in certification of the ground truth. To that end, we experiment with `orientation` and `scale` as the continuous sensitive attributes which have $v = 15$ and $v = 8$ different possible values respectively. In particular, $v = 15$ for `orientation` is the most among all latent factors, and thus provides for the most rigorous evaluation. The rest of the generative factors are either hue or shape, which are discrete. We set the target attribute to `object hue`, which has 10 different classes.

For each of the selected sensitive attributes, we filter the original training set to create a biased one, correlating the sensitive and the target attributes. We only keep those samples in the training set for which: (i) $\text{hue} \leq 5$ and $\text{orient} \leq 7 / \text{scale} \leq 4$, or (ii) $\text{hue} \geq 6$ and $\text{orient} \geq 9 / \text{scale} \geq 5$. We extend the attribute vector computation (performed on the original, unfiltered training set) to non-binary attributes, defining $a_{ij} = z_{G,i} - z_{G,j}$, where $1 \leq i, j \leq v$ are sensitive attribute values. Based on the construction of the biased training set, we let the similarity set $S(\mathbf{x})$ to be defined by all attribute vectors $\{a_{ij}\}$ for which $i < 8 < j$ for `orientation` ($7 \cdot 7 = 49$ vectors) and $i \leq 4 < j$ for `scale` ($4 \cdot 4 = 16$ vectors) and $\epsilon = 1$.

In the evaluation, apart from reporting the accuracy and the certified fairness on the (unbiased) test subset, for each sample we also obtain the v similar ground truth data points, i.e., the same shape at v different orientations (or scales, depending on the sensitive attribute), while fixing all other factors. Then, if any of the v similar data points is certified, we check whether all v similar ground truth data points obtain the same classification, indicating ground truth fairness.

The results in Tab. 5 indicate that LASSI substantially increases the accuracy and the certified individual fairness (w.r.t. the similarity sets computed using Glow), while being nearly 100% empirically fair on the ground truth images. That is, in only 0.3% (for `orientation`) and 2.7% (for `scale`) of the test samples there were different classification

Table 5: Evaluation on 3D Shapes for the task object hue. Certification with the generative model transfers to ground truth data as the certification rate and the percentage of empirically unfair ground truth data sum up below 100%.

Method:	Naive			LASSI (ours)		
	Sensitive attribute	Acc	Cert. Fair	Emp. Unfair (\downarrow)	Acc	Cert. Fair
orientation	32.0	0	69.3	100	81.3	0.3
scale	80.3	0	20.3	95.0	69.3	2.7

outcomes among their v similar (ground-truth) samples. Crucially, in all of these cases, our method did not certify individual fairness for *any* of these v similar data points, showing that the certificates transfer to the ground truth.

6 Limitations and Future Work

We now discuss some of the limitations of LASSI. First, our method trains individually fair models, but it does not guarantee that models satisfy other fairness notions, e.g., group fairness. While individual fairness is a well-studied research area, recent work argues that it does not qualify as a valid fairness notion as it can be insufficient to guarantee fairness in certain instances and risks encoding implicit human biases [87]. Moreover, the validity of our fairness certificates depends heavily on the generative model used by LASSI. In particular, the similarity sets $S(\mathbf{x})$ considered in our work may not be exhaustive enough as there can be latent points outside $S(\mathbf{x})$ that correspond to input points that would be perceived as similar to \mathbf{x} by a human observer. This can also happen if the generative model is not powerful enough to generate all possible instances and combinations of similar individuals. For the above reasons, it is hard to obtain formal guarantees about G and the computed certificates may not always transfer from G to the real world. Future work can consider mitigating these issues by performing extensive manual human inspection of reconstructions produced by G (similar to App. E). Moreover, all future advancements in the active research area of normalizing flows will immediately improve the quality of our certificates.

7 Conclusion

We proposed LASSI, which defines image similarity with respect to a generative model via attribute manipulation, allowing us to capture complex image transformations such as changing the age or skin color, which are otherwise difficult to characterize. Further, we were able to scale certified representation learning for individual fairness to real-world high-dimensional datasets by using randomized smoothing-based techniques. Our extensive evaluation yields promising results on several datasets and illustrates the practicality of our approach.

Ethics Statement

In this work, we proposed a novel method for certifying the individual fairness of models operating on high-dimensional data. Progress on this challenging problem could enable fairness auditing for high-risk computer vision applications, such as facial recognition. Stark [88] argues that facial recognition and analysis algorithms can have undesirable, socially toxic, and divisive consequences. For instance, it has been demonstrated that they may perpetuate and reinforce racial and gender bias [4, 57]. Therefore, their applications must be carefully considered, including the social dynamics and context in which they occur. Accordingly, following prior work [57], we refrained from using unstable social constructs, such as gender, or normatively judgemental attributes, such as “attractive” or “chubby”, in our research.

One way to limit the potential harms of facial analysis technologies is to control and regulate their usage. Our work aims to help fill this gap by presenting a methodology for enforcing individual fairness via certification. As highlighted in our paper, we acknowledge that the quality of the generative models is a significant bottleneck of our certificates. For example, they may encode various biases present in the data. Another possible source of bias is the human perception and social constructs which can potentially impact the validity of our similarity specifications. Nevertheless, we believe that we can still leverage generative models and their latent space to construct more meaningful individual fairness specifications on high-dimensional data than those allowed by prior work. More broadly speaking, developing rigorous, standardized processes for auditing and certifying facial recognition models (including human inspection, e.g., by considering the reconstructed images in our appendix) should complement the contributions presented in our work. Finally, future quality advancements in generative modelling and normalizing flows can directly translate into stronger guarantees of our method, enabling certified fair application of models using rich, high-dimensional data.

Acknowledgments

We would like to thank Seyedmorteza Sadat for his help with initial investigations in enforcing fairness in the latent space of a generative model. We are also grateful to the anonymous reviewers for their insightful comments and suggestions.

References

- [1] Xudong Sun, Pengcheng Wu, and Steven C. H. Hoi. Face detection using deep learning: An improved faster RCNN approach. *Neurocomputing*, 2018. 1
- [2] Amir E. Khandani, Adlar J. Kim, and Andrew W. Lo. Consumer credit-risk models via machine-learning algorithms. *Journal of Banking & Finance*, 2010. 1
- [3] Tim Brennan, William Dieterich, and Beate Ehret. Evaluating the predictive validity of the compas risk and needs assessment system. *Criminal Justice and Behavior*, 2009. 1
- [4] Joy Buolamwini and Timnit Gebru. Gender shades: Intersectional accuracy disparities in commercial gender classification. In *Conference on Fairness, Accountability and Transparency*, 2018. 1, 3, 10
- [5] Brendan Klare, Mark James Burge, Joshua C. Klontz, Richard W. Vorder Bruegge, and Anil K. Jain. Face recognition performance: Role of demographic information. *IEEE Trans. Inf. Forensics Secur.*, 2012. 1, 3
- [6] EU. Ethics guidelines for trustworthy ai, 2019. 1, 3
- [7] EU. Proposal for a regulation of the european parliament and of the council laying down harmonised rules on artificial intelligence (artificial intelligence act) and amending certain union legislative acts, 2021.
- [8] FTC. Using artificial intelligence and algorithms, 2020.
- [9] FTC. Aiming for truth, fairness, and equity in your company's use of ai, 2021.
- [10] UN. The right to privacy in the digital age, 2021. 1, 3
- [11] Richard S. Zemel, Yu Wu, Kevin Swersky, Toniann Pitassi, and Cynthia Dwork. Learning fair representations. In *Proceedings of the 30th International Conference on Machine Learning*, 2013. 1, 3
- [12] Daniel McNamara, Cheng Soon Ong, and Robert C. Williamson. Costs and benefits of fair representation learning. In *Proceedings of the 2019 AAAI/ACM Conference on AI, Ethics, and Society*, 2019. 1
- [13] Xavier Gitiaux and Huzefa Rangwala. Learning smooth and fair representations. In *The 24th International Conference on Artificial Intelligence and Statistics*, 2021. 1, 3
- [14] Anian Ruoss, Mislav Balunovic, Marc Fischer, and Martin T. Vechev. Learning certified individually fair representations. In *Advances in Neural Information Processing Systems 33*, 2020. 1, 2, 3, 4, 5, 7
- [15] Mikhail Yurochkin, Amanda Bower, and Yuekai Sun. Training individually fair ML models with sensitive subspace robustness. In *8th International Conference on Learning Representations*, 2020. 1, 3
- [16] Samuel Yeom and Matt Fredrikson. Individual fairness revisited: Transferring techniques from adversarial robustness. In *Proceedings of the Twenty-Ninth International Joint Conference on Artificial Intelligence*, 2020. 2, 3
- [17] Rüdiger Ehlers. Formal verification of piece-wise linear feed-forward neural networks. In *Automated Technology for Verification and Analysis - 15th International Symposium*, 2017. 2, 4
- [18] Vincent Tjeng, Kai Yuanqing Xiao, and Russ Tedrake. Evaluating robustness of neural networks with mixed integer programming. In *7th International Conference on Learning Representations*, 2019. 2, 4
- [19] Diederik P. Kingma and Prafulla Dhariwal. Glow: Generative flow with invertible 1x1 convolutions. In *Advances in Neural Information Processing Systems 31*, 2018. 2, 4
- [20] Jeremy M. Cohen, Elan Rosenfeld, and J. Zico Kolter. Certified adversarial robustness via randomized smoothing. In *Proceedings of the 36th International Conference on Machine Learning*, 2019. 2, 4, 5, 6, 16, 19
- [21] Aounon Kumar and Tom Goldstein. Center smoothing: Certified robustness for networks with structured outputs. *Advances in Neural Information Processing Systems 34*, 2021. 2, 4, 5, 6, 16, 19
- [22] Cynthia Dwork, Moritz Hardt, Toniann Pitassi, Omer Reingold, and Richard S. Zemel. Fairness through awareness. In *Innovations in Theoretical Computer Science*, 2012. 3

[23] Moritz Hardt, Eric Price, and Nati Srebro. Equality of opportunity in supervised learning. In *Advances in Neural Information Processing Systems 29*, 2016. 3

[24] Michael J. Kearns, Seth Neel, Aaron Roth, and Zhiwei Steven Wu. Preventing fairness gerrymandering: Auditing and learning for subgroup fairness. In *Proceedings of the 35th International Conference on Machine Learning*, 2018. 3

[25] Christina Ilvento. Metric learning for individual fairness. In *1st Symposium on Foundations of Responsible Computing*, 2020. 3

[26] Subha Maity, Songkai Xue, Mikhail Yurochkin, and Yuekai Sun. Statistical inference for individual fairness. In *9th International Conference on Learning Representations*, 2021.

[27] Debarghya Mukherjee, Mikhail Yurochkin, Moulinath Banerjee, and Yuekai Sun. Two simple ways to learn individual fairness metrics from data. In *Proceedings of the 37th International Conference on Machine Learning*, 2020.

[28] Hanchen Wang, Nina Grgic-Hlaca, Preethi Lahoti, Krishna P. Gummadi, and Adrian Weller. An empirical study on learning fairness metrics for COMPAS data with human supervision. *CoRR*, 2019.

[29] Mikhail Yurochkin and Yuekai Sun. Sensei: Sensitive set invariance for enforcing individual fairness. In *9th International Conference on Learning Representations*, 2021. 3

[30] Harrison Edwards and Amos J. Storkey. Censoring representations with an adversary. In *4th International Conference on Learning Representations*, 2016. 3

[31] Thomas Kehrenberg, Myles Bartlett, Oliver Thomas, and Novi Quadrianto. Null-sampling for interpretable and fair representations. In *Computer Vision - ECCV 2020 - 16th European Conference*, 2020.

[32] Jiachun Liao, Chong Huang, Peter Kairouz, and Lalitha Sankar. Learning generative adversarial representations (GAP) under fairness and censoring constraints. *CoRR*, 2019.

[33] David Madras, Elliot Creager, Toniann Pitassi, and Richard S. Zemel. Learning adversarially fair and transferable representations. In *Proceedings of the 35th International Conference on Machine Learning*, 2018. 3, 5, 8

[34] Elliot Creager, David Madras, Jörn-Henrik Jacobsen, Marissa A. Weis, Kevin Swersky, Toniann Pitassi, and Richard S. Zemel. Flexibly fair representation learning by disentanglement. In *Proceedings of the 36th International Conference on Machine Learning*, 2019. 3

[35] Francesco Locatello, Gabriele Abbati, Thomas Rainforth, Stefan Bauer, Bernhard Schölkopf, and Olivier Bachem. On the fairness of disentangled representations. In *Advances in Neural Information Processing Systems 32*, 2019. 6

[36] Mhd Hasan Sarhan, Nassir Navab, Abouzar Eslami, and Shadi Albarqouni. Fairness by learning orthogonal disentangled representations. In *Computer Vision - ECCV 2020 - 16th European Conference*, 2020. 3

[37] Jiaming Song, Pratyusha Kalluri, Aditya Grover, Shengjia Zhao, and Stefano Ermon. Learning controllable fair representations. In *The 22nd International Conference on Artificial Intelligence and Statistics*, 2019. 3

[38] Luca Oneto, Michele Donini, Massimiliano Pontil, and Andreas Maurer. Learning fair and transferable representations with theoretical guarantees. In *7th IEEE International Conference on Data Science and Advanced Analytics*, 2020. 3

[39] Mislav Balunovic, Anian Ruoss, and Martin T. Vechev. Fair normalizing flows. *CoRR*, 2021. 3

[40] Christos Louizos, Kevin Swersky, Yujia Li, Max Welling, and Richard S. Zemel. The variational fair autoencoder. In *4th International Conference on Learning Representations*, 2016.

[41] Han Zhao, Amanda Coston, Tameem Adel, and Geoffrey J. Gordon. Conditional learning of fair representations. In *8th International Conference on Learning Representations*, 2020. 3

[42] Rui Feng, Yang Yang, Yuehan Lyu, Chenhao Tan, Yizhou Sun, and Chunping Wang. Learning fair representations via an adversarial framework. *CoRR*, 2019. 3

[43] Preethi Lahoti, Krishna P. Gummadi, and Gerhard Weikum. ifair: Learning individually fair data representations for algorithmic decision making. In *35th IEEE International Conference on Data Engineering*, 2019. 3

[44] Preethi Lahoti, Krishna P. Gummadi, and Gerhard Weikum. Operationalizing individual fairness with pairwise fair representations. *Proc. VLDB Endow.*, 2019. 3

[45] Zeyu Wang, Klint Qinami, Ioannis Christos Karakozis, Kyle Genova, Prem Nair, Kenji Hata, and Olga Russakovsky. Towards fairness in visual recognition: Effective strategies for bias mitigation. In *IEEE/CVF Conference on Computer Vision and Pattern Recognition*, 2020. 3

[46] Benjamin Wilson, Judy Hoffman, and Jamie Morgenstern. Predictive inequity in object detection. *CoRR*, 2019. 3

[47] Tolga Bolukbasi, Kai-Wei Chang, James Y. Zou, Venkatesh Saligrama, and Adam Tauman Kalai. Man is to computer programmer as woman is to homemaker? debiasing word embeddings. In *Advances in Neural Information Processing Systems 29*, 2016. 3

[48] Paul Pu Liang, Chiyu Wu, Louis-Philippe Morency, and Ruslan Salakhutdinov. Towards understanding and mitigating social biases in language models. In *Proceedings of the 38th International Conference on Machine Learning*, 2021.

[49] Ji Ho Park, Jamin Shin, and Pascale Fung. Reducing gender bias in abusive language detection. In *Proceedings of the 2018 Conference on Empirical Methods in Natural Language Processing*, 2018.

[50] Rachael Tatman. Gender and dialect bias in youtube's automatic captions. In *Proceedings of the First ACL Workshop on Ethics in Natural Language Processing*, 2017. 3

[51] Inioluwa Deborah Raji and Joy Buolamwini. Actionable auditing: Investigating the impact of publicly naming biased performance results of commercial AI products. In *Proceedings of the 2019 AAAI/ACM Conference on AI, Ethics, and Society*, 2019. 3

[52] Lisa Anne Hendricks, Kaylee Burns, Kate Saenko, Trevor Darrell, and Anna Rohrbach. Women also snowboard: Overcoming bias in captioning models. In *Computer Vision - ECCV 2018 - 15th European Conference*, 2018. 3

[53] Jieyu Zhao, Tianlu Wang, Mark Yatskar, Vicente Ordonez, and Kai-Wei Chang. Men also like shopping: Reducing gender bias amplification using corpus-level constraints. In *Proceedings of the 2017 Conference on Empirical Methods in Natural Language Processing*, 2017. 3

[54] Tianlu Wang, Jieyu Zhao, Mark Yatskar, Kai-Wei Chang, and Vicente Ordonez. Balanced datasets are not enough: Estimating and mitigating gender bias in deep image representations. In *IEEE/CVF International Conference on Computer Vision*, 2019. 3

[55] Guha Balakrishnan, Yuanjun Xiong, Wei Xia, and Pietro Perona. Towards causal benchmarking of bias in face analysis algorithms. In *Computer Vision - ECCV 2020 - 16th European Conference*, 2020. 3, 4

[56] Saloni Dash and Amit Sharma. Counterfactual generation and fairness evaluation using adversarially learned inference. *CoRR*, 2020.

[57] Emily Denton, Ben Hutchinson, Margaret Mitchell, and Timnit Gebru. Detecting bias with generative counterfactual face attribute augmentation. *CoRR*, 2019. 4, 6, 7, 8, 10, 19

[58] Jungseock Joo and Kimmo Kärkkäinen. Gender slopes: Counterfactual fairness for computer vision models by attribute manipulation. *CoRR*, 2020.

[59] Been Kim, Martin Wattenberg, Justin Gilmer, Carrie J. Cai, James Wexler, Fernanda B. Viégas, and Rory Sayres. Interpretability beyond feature attribution: Quantitative testing with concept activation vectors (TCAV). In *Proceedings of the 35th International Conference on Machine Learning*, 2018. 4

[60] Hyemi Kim, Seungjae Shin, JoonHo Jang, Kyungwoo Song, Weonyoung Joo, Wanmo Kang, and Il-Chul Moon. Counterfactual fairness with disentangled causal effect variational autoencoder. In *Thirty-Fifth AAAI Conference on Artificial Intelligence*, 2021.

[61] Vikram V. Ramaswamy, Sunnie S. Y. Kim, and Olga Russakovsky. Fair attribute classification through latent space de-biasing. In *IEEE Conference on Computer Vision and Pattern Recognition*, 2021. 4, 6, 7, 8, 21, 22

[62] Prasanna Sattigeri, Samuel C. Hoffman, Vijil Chenthamarakshan, and Kush R. Varshney. Fairness GAN: generating datasets with fairness properties using a generative adversarial network. *IBM J. Res. Dev.*, 2019. 3

[63] Daniel J. McDuff, Roger Cheng, and Ashish Kapoor. Identifying bias in AI using simulation. *CoRR*, 2018. 3

[64] Sven Gowal, Chongli Qin, Po-Sen Huang, A. Taylan Cemgil, Krishnamurthy Dvijotham, Timothy A. Mann, and Pushmeet Kohli. Achieving robustness in the wild via adversarial mixing with disentangled representations. In *IEEE/CVF Conference on Computer Vision and Pattern Recognition*, 2020. 3

[65] Eric Wong and J. Zico Kolter. Learning perturbation sets for robust machine learning. In *9th International Conference on Learning Representations*, 2021. 3

[66] Matthew Mirman, Alexander Hägele, Pavol Bielik, Timon Gehr, and Martin T. Vechev. Robustness certification with generative models. In *42nd ACM SIGPLAN International Conference on Programming Language Design and Implementation*, 2021. 3

[67] Aws Albarghouthi, Loris D’Antoni, Samuel Drews, and Aditya V. Nori. Fairsquare: probabilistic verification of program fairness. *Proc. ACM Program. Lang.*, 2017. 3

[68] Osbert Bastani, Xin Zhang, and Armando Solar-Lezama. Probabilistic verification of fairness properties via concentration. *Proc. ACM Program. Lang.*, 2019.

[69] YooJung Choi, Meihua Dang, and Guy Van den Broeck. Group fairness by probabilistic modeling with latent fair decisions. In *Thirty-Fifth AAAI Conference on Artificial Intelligence*, 2021.

[70] Shahar Segal, Yossi Adi, Benny Pinkas, Carsten Baum, Chaya Ganesh, and Joseph Keshet. Fairness in the eyes of the data: Certifying machine-learning models. In *AAAI/ACM Conference on AI, Ethics, and Society*, 2021. 3

[71] Philips George John, Deepak Vijaykeerthy, and Diptikalyan Saha. Verifying individual fairness in machine learning models. In *Proceedings of the Thirty-Sixth Conference on Uncertainty in Artificial Intelligence*, 2020. 3

[72] Caterina Urban, Maria Christakis, Valentin Wüstholtz, and Fuyuan Zhang. Perfectly parallel fairness certification of neural networks. *Proc. ACM Program. Lang.*, 2020. 3

[73] Ian J. Goodfellow, Jean Pouget-Abadie, Mehdi Mirza, Bing Xu, David Warde-Farley, Sherjil Ozair, Aaron C. Courville, and Yoshua Bengio. Generative adversarial nets. In *Advances in Neural Information Processing Systems 27*, 2014. 4, 6

[74] Diederik P. Kingma and Max Welling. Auto-encoding variational bayes. In *2nd International Conference on Learning Representations*, 2014. 4

[75] Irina Higgins, Loïc Matthey, Arka Pal, Christopher Burgess, Xavier Glorot, Matthew Botvinick, Shakir Mohamed, and Alexander Lerchner. beta-vae: Learning basic visual concepts with a constrained variational framework. In *5th International Conference on Learning Representations*, 2017. 4

[76] Aleksander Madry, Aleksandar Makelov, Ludwig Schmidt, Dimitris Tsipras, and Adrian Vladu. Towards deep learning models resistant to adversarial attacks. In *6th International Conference on Learning Representations*, 2018. 5

[77] Logan Engstrom, Brandon Tran, Dimitris Tsipras, Ludwig Schmidt, and Aleksander Madry. Exploring the landscape of spatial robustness. In *Proceedings of the 36th International Conference on Machine Learning*, 2019. 5

[78] Ian J. Goodfellow, Jonathon Shlens, and Christian Szegedy. Explaining and harnessing adversarial examples. In *3rd International Conference on Learning Representations*, 2015. 5

[79] Xi Lin, Hui-Ling Zhen, Zhenhua Li, Qingfu Zhang, and Sam Kwong. Pareto multi-task learning. In *Advances in Neural Information Processing Systems 32*, 2019. 5

[80] Natalia Martínez, Martín Bertrán, and Guillermo Sapiro. Minimax pareto fairness: A multi objective perspective. In *Proceedings of the 37th International Conference on Machine Learning*, 2020.

[81] Susan Wei and Marc Niethammer. The fairness-accuracy pareto front. *CoRR*, 2020. 5

[82] Ziwei Liu, Ping Luo, Xiaogang Wang, and Xiaoou Tang. Deep learning face attributes in the wild. In *IEEE International Conference on Computer Vision*, 2015. 6, 17

[83] Kimmo Kärkkäinen and Jungseock Joo. Fairface: Face attribute dataset for balanced race, gender, and age for bias measurement and mitigation. In *IEEE Winter Conference on Applications of Computer Vision*, 2021. 6, 9, 17

[84] Chris Burgess and Hyunjik Kim. 3d shapes dataset. <https://github.com/deepmind/3dshapes-dataset/>, 2018. 6, 9

[85] Adam Paszke, Sam Gross, Francisco Massa, Adam Lerer, James Bradbury, Gregory Chanan, Trevor Killeen, Zeming Lin, Natalia Gimelshein, Luca Antiga, Alban Desmaison, Andreas Köpf, Edward Z. Yang, Zachary DeVito, Martin Raison, Alykhan Tejani, Sasank Chilamkurthy, Benoit Steiner, Lu Fang, Junjie Bai, and Soumith Chintala. Pytorch: An imperative style, high-performance deep learning library. In Hanna M. Wallach, Hugo

Larochelle, Alina Beygelzimer, Florence d’Alché-Buc, Emily B. Fox, and Roman Garnett, editors, *Advances in Neural Information Processing Systems 32*, 2019. 6

- [86] Kim Seonghyeon. Glow pytorch (commit: 97081ff1). <https://github.com/rosinality/glow-pytorch>, 2020. 6
- [87] Will Fleisher. What’s fair about individual fairness? In *AAAI/ACM Conference on AI, Ethics, and Society, Virtual Event*, 2021. 10
- [88] Luke Stark. Facial recognition is the plutonium of ai. *XRDS*, 25(3):50–55, apr 2019. ISSN 1528-4972. doi: 10.1145/3313129. URL <https://doi.org/10.1145/3313129>. 10

A Proof of Thm. 4.1

This section provides a formal proof of the following:

Theorem 4.1. *Assume that we have a bijective generative model $G = D \circ E$ used to define the similarity set $S_i(\mathbf{x})$ for a given input \mathbf{x} . Let Alg. 1 perform center smoothing [21] with confidence $1 - \alpha_{cs}$ and randomized smoothing [20] with confidence $1 - \alpha_{rs}$. If Alg. 1 returns CERTIFIED for the input \mathbf{x} , then the end-to-end model $M = \widehat{C} \circ \widehat{R} \circ E$ is individually fair for \mathbf{x} with respect to $S_i(\mathbf{x})$ with probability at least $1 - \alpha_{cs} - \alpha_{rs}$.*

To prove Thm. 4.1, we will make use of the following randomized and center smoothing theorems proved in the literature:

Theorem A.1 (Adapted from [20]). *Let $C : \mathbb{R}^k \mapsto \mathcal{Y}$ be a classifier and let $\varepsilon \sim \mathcal{N}(0, \sigma_{rs}^2 I)$. Let \widehat{C} be defined such that $\widehat{C}(\mathbf{r}) = \arg \max_{c \in \mathcal{Y}} \mathbb{P}_\varepsilon(C(\mathbf{r} + \varepsilon) = c)$. Suppose $c_A \in \mathcal{Y}$ and $\underline{p}_A, \overline{p}_B \in [0, 1]$ satisfy:*

$$\mathbb{P}_\varepsilon(C(\mathbf{r} + \varepsilon) = c_A) \geq \underline{p}_A \geq \overline{p}_B \geq \max_{c_B \neq c_A} \mathbb{P}_\varepsilon(C(\mathbf{r} + \varepsilon) = c_B). \quad (7)$$

Then $\widehat{C}(\mathbf{r} + \delta) = c_A$ for all δ satisfying $\|\delta\|_2 < d_{rs}$, where $d_{rs} := \frac{\sigma_{rs}}{2} (\Phi^{-1}(\underline{p}_A) - \Phi^{-1}(\overline{p}_B))$.

Here, \mathcal{Y} denotes the set of class labels, Φ is the cumulative distribution function (CDF) of the standard normal distribution $\mathcal{N}(0, 1)$, and Φ^{-1} is its inverse.

Theorem A.2 (Adapted from [21]). *Let $g : \mathbb{R}^a \mapsto \mathbb{R}^k$ and $\hat{g} : \mathbb{R}^a \mapsto \mathbb{R}^k$ is an approximation of the smoothed version of g , which maps $\mathbf{t} \in \mathbb{R}^a$ to the center point $\hat{g}(\mathbf{t})$ of a minimum enclosing ball containing at least half of the points $\mathbf{r}_i \sim g(\mathbf{t} + \mathcal{N}(0, \sigma_{cs}^2 I))$, $i \in \{1, \dots, m\}$. Then, for $\epsilon > 0$, with probability at least $1 - \alpha_{cs}$ we have,*

$$\forall \mathbf{t}' \text{ s.t. } \|\mathbf{t} - \mathbf{t}'\|_2 \leq \epsilon, \|\hat{g}(\mathbf{t}) - \hat{g}(\mathbf{t}')\|_2 \leq d_{cs}. \quad (8)$$

We now proceed to proving Thm. 4.1:

Proof. Assume that Alg. 1 returns CERTIFIED for the input \mathbf{x} . We need to show that with high probability

$$\forall \mathbf{x}' \in S_i(\mathbf{x}) : M(\mathbf{x}) = M(\mathbf{x}'). \quad (\text{Eq. 6})$$

By definition of $S_i(\mathbf{x})$, it follows that for all $\mathbf{x}' \in S_i(\mathbf{x})$, there exists a $\mathbf{z}' \in S(\mathbf{x})$ such that $\mathbf{x}' = D(\mathbf{z}')$. By assumption, G is bijective, so $\mathbf{z}' = E(\mathbf{x}')$. That is, for all $\mathbf{x}' \in S_i(\mathbf{x})$, passing \mathbf{x}' through the first component of the model M (namely, E) results in a point $\mathbf{z}' \in S(\mathbf{x})$.

As G and \mathbf{x} are given, we compute $\mathbf{z}_G = E(\mathbf{x})$. To prove the statement in Eq. (6), we now need to show that with high probability

$$\forall \mathbf{z}' \in S(\mathbf{x}) : (\widehat{C} \circ \widehat{R})(\mathbf{z}_G) = (\widehat{C} \circ \widehat{R})(\mathbf{z}'). \quad (9)$$

The next step of the model pipeline computes $\widehat{R}(\mathbf{z})$ for a $\mathbf{z} \in \mathbb{R}^q$ in the latent space of the generative model G . Recall that \widehat{R} was defined such that $\widehat{R}(\mathbf{z}) = \widehat{g}_z(0)$, where $\widehat{g}_z(0)$ is the output of the center smoothed [21] function $g_z(t) = R(\mathbf{z} + t \cdot \mathbf{a})$, $t \in \mathbb{R}$ at $t = 0$. Note that if $\mathbf{z}' = \mathbf{z} + t' \cdot \mathbf{a}$, then

$$\begin{aligned} g_{\mathbf{z}'}(t) &= R(\mathbf{z}' + t \cdot \mathbf{a}) \\ &= R(\mathbf{z} + t' \cdot \mathbf{a} + t \cdot \mathbf{a}) \\ &= R(\mathbf{z} + (t + t') \cdot \mathbf{a}) \\ &= g_{\mathbf{z}}(t + t') \end{aligned} \quad (10)$$

That is, $g_{\mathbf{z}'}(t) = g_{\mathbf{z}}(t + t')$, which implies $\widehat{g}_{\mathbf{z}'}(t) = \widehat{g}_{\mathbf{z}}(t + t')$, and in particular $\widehat{R}(\mathbf{z}') = \widehat{g}_{\mathbf{z}'}(0) = \widehat{g}_{\mathbf{z}}(t')$.

Now, let us get back to Eq. (9). For all $\mathbf{z}' \in S(\mathbf{x})$, by definition of $S(\mathbf{x})$, $\mathbf{z}' = \mathbf{z}_G + t' \cdot \mathbf{a}$ for some $t' \in [-\epsilon, \epsilon]$. Moreover, $\mathbf{r}_{cs} = \widehat{R}(\mathbf{z}_G) = \widehat{g}_{\mathbf{z}_G}(0)$ and $\widehat{R}(\mathbf{z}') = \widehat{g}_{\mathbf{z}_G}(t')$. Thm. A.2 tells us that with probability at least $1 - \alpha_{cs}$

$$\begin{aligned} \forall t' \in [-\epsilon, \epsilon] : \|\widehat{g}_{\mathbf{z}_G}(0) - \widehat{g}_{\mathbf{z}_G}(t')\|_2 &\leq d_{cs} \\ \iff \forall \mathbf{z}' \in S(\mathbf{x}) : \|\mathbf{r}_{cs} - \widehat{R}(\mathbf{z}')\|_2 &\leq d_{cs}, \end{aligned} \quad (11)$$

provided that the center smoothing computation of \mathbf{r}_{cs} does not abstain.

Table 6: Sensitive attribute statistics. As the attribute vectors are computed using the training data, the positive and negative sample ratio is reported for the training set (except for 3D Shapes where the attributes are not binary). For 3D Shapes, we report the average length of all vectors associated with the corresponding attribute.

Dataset	Sensitive attribute	Pos (%)	Neg (%)	$\ z_{G, \text{pos}} - z_{G, \text{neg}}\ _2$
CelebA	Pale_Skin	4.3	95.7	11.5
	Young	77.9	22.1	7.8
	Blond_Hair	14.9	85.1	15.8
	Heavy_Makeup	38.4	61.6	11.9
FairFace	Race=Black	14.1	85.9	10.9
3D Shapes	orientation	—	—	56.9
	scale	—	—	35.5

Table 7: Baseline accuracies for the Smiling and Earrings CelebA tasks. The ResNet-18 classifier takes the original images as an input, while the z_G classifier is a fully connected network classifying their Glow latent representations. Neither of these classifiers involves representation learning.

Task	Majority class		Acc (ResNet-18)		Acc (z_G)	
	Valid	Test	Valid	Test	Valid	Test
Smiling	51.7	52.6	92.1 ± 0.2	90.9 ± 0.7	89.4 ± 0.1	87.2 ± 1.1
Earrings	80.9	78.2	86.2 ± 0.8	88.2 ± 1.1	84.7 ± 0.1	85.2 ± 0.9

Now, we consider the final component of the pipeline – the smoothed classifier \widehat{C} . Provided that \widehat{C} does not abstain at the input r_{cs} , Thm. A.1 provides us with a radius d_{rs} around r_{cs} such that with probability at least $1 - \alpha_{rs}$

$$\begin{aligned} \forall \delta \text{ s.t. } \|\delta\|_2 < d_{rs}, \quad \widehat{C}(r_{cs}) &= \widehat{C}(r_{cs} + \delta) \\ \iff \forall r' \text{ s.t. } \|r_{cs} - r'\|_2 < d_{rs}, \quad \widehat{C}(r_{cs}) &= \widehat{C}(r'). \end{aligned} \quad (12)$$

If Alg. 1 returns CERTIFIED, that is $d_{cs} < d_{rs}$, combining Eq. (11) and (12) and applying the union bound, we obtain that with probability at least $1 - \alpha_{cs} - \alpha_{rs}$ we have $\widehat{C}(r_{cs}) = \widehat{C}(\widehat{R}(z'))$ for all $z' \in S(\mathbf{x})$. That is,

$$\forall z' \in S(\mathbf{x}) : (\widehat{C} \circ \widehat{R})(z_G) = (\widehat{C} \circ \widehat{R})(z'), \quad (13)$$

as required by Eq. (9). The same proof technique can also be extended to the multiple attribute vectors case. \square

B Datasets and Dataset Statistics

In this section we provide further information and statistics about the datasets used in this work. CelebA² [82] is restricted to non-commercial research and education purposes and its authors [82] do not own the copyrights. FairFace [83] is licensed under CC BY 4.0 and the license of 3D Shapes is Apache-2.0. Tab. 6 contains statistics about the sensitive attributes and their corresponding attribute vectors. The lengths of the CelebA attribute vectors are computed for 64×64 images.

In Tab. 7 we report the base accuracies of two standard classifiers trained on the Smiling and Earrings CelebA tasks. The first classifier is a ResNet-18 network trained directly on the original images. The other one is a fully connected network operating on their Glow latent representations, $z_G = E(\mathbf{x})$. We remark that none of these classifiers involves representation learning. We report the means and standard deviations, averaged over 5 runs with different random seeds, on the validation and test sets, where the test set is the same subset on which we report the results in the main paper. The base accuracies on the downstream tasks used for the transfer learning experiments are reported in App. D.

In order to estimate the relative “unfairness” associated with each sensitive attribute, in Tab. 8 we compute the empirical individual fairness of the two classifiers. For each data point \mathbf{x} , we sample 9 points from $S_i(\mathbf{x})$ evenly (15 points for Pale+Young+Blond). If all samples are classified the same, we add the original data point \mathbf{x} to the empirical fairness counter. Note that this procedure cannot certify that all points from $S_i(\mathbf{x})$ are classified the same. Therefore, these results come with no provable guarantees and serve as upper bounds of the certified individual fairness of the classifiers.

²<https://mmlab.ie.cuhk.edu.hk/projects/CelebA.html>

Table 8: Empirical individual fairness of the base classifiers evaluated via sampling. These results come with no provable guarantees and serve as upper bounds of the certified individual fairness.

Task	Sensitive attribute(s)	Emp. Fair (ResNet-18)		Emp. Fair (z_G)	
		Valid	Test	Valid	Test
Smiling	Pale_Skin	74.1 \pm 1.0	75.2 \pm 1.1	75.8 \pm 0.6	79.9 \pm 1.2
	Young	87.7 \pm 0.5	90.1 \pm 0.7	95.2 \pm 0.6	96.8 \pm 0.9
	Blond_Hair	89.1 \pm 1.1	89.4 \pm 1.5	81.9 \pm 1.6	84.6 \pm 2.9
	Heavy_Makeup	82.3 \pm 1.0	82.5 \pm 1.2	74.9 \pm 1.6	78.2 \pm 2.3
	Pale+Young	71.5 \pm 0.9	72.6 \pm 1.1	75.8 \pm 0.6	79.9 \pm 1.2
	Pale+Young+Blond	70.3 \pm 0.5	70.6 \pm 0.9	72.5 \pm 0.6	76.9 \pm 1.1
Earrings	Pale_Skin	92.8 \pm 0.9	90.4 \pm 1.2	91.5 \pm 1.0	91.5 \pm 1.6
	Young	90.6 \pm 1.8	87.7 \pm 1.5	93.0 \pm 1.2	94.7 \pm 1.0
	Blond_Hair	89.7 \pm 2.2	86.9 \pm 2.5	88.3 \pm 1.9	89.7 \pm 2.2
	Heavy_Makeup	85.8 \pm 3.4	82.2 \pm 3.3	74.4 \pm 4.4	73.3 \pm 3.8

Table 9: Results of Naive on the validation subset of CelebA for different values of σ_{cs} and σ_{rs} . The third column contains the mean center smoothing radii corresponding to the different σ_{cs} values. Smaller is generally better for certified individual fairness (see the condition in Alg. 1).

Sens. attribute	σ_{cs}	Mean d_{cs}	Metric	σ_{rs}							
				0.1	0.25	0.5	1	2.5	5	10	25
Pale_Skin	0.5	42.25	Acc	87.8	87.8	87.5	88.4	89.1	88.7	88.7	84.6
			Fair	0	0	0	0	0	0	0	0
	0.55	34.19	Acc	87.8	87.8	87.8	88.4	88.7	88.7	88.4	84.6
			Fair	0	0	0	0	0	0	0	0
	0.6	33.34	Acc	87.8	87.5	87.8	88.4	88.7	88.7	88.7	84.6
			Fair	0	0	0	0	0	0	1.0	0
Young	0.65	33.37	Acc	87.5	87.5	87.8	88.4	88.8	88.7	88.4	84.6
			Fair	0	0	0	0	0	0	1.0	0
	0.7	33.72	Acc	87.5	87.5	87.5	88.4	88.4	88.7	88.1	84.6
			Fair	0	0	0	0	0	0	1.0	0
	0.75	34.18	Acc	87.8	88.1	88.1	88.4	88.7	89.1	88.1	84.6
			Fair	0	0	0	0	0	0	1.0	0
	0.6	8.16	Acc	88.1	88.1	87.8	87.8	88.7	88.7	88.1	85.2
			Fair	0	0	0	5.1	36.3	58.8	58.5	39.9
	0.65	8.16	Acc	88.1	88.1	87.8	87.8	88.7	88.7	88.1	84.9
			Fair	0	0	0	4.8	36.3	58.8	58.2	39.5

C Hyperparameter Tuning

In this section, we perform an extensive hyperparameter search in order to select suitable values for the hyperparameters. We evaluate on 311 samples from the *validation* set of CelebA (again, every 64-th), on the Smiling task with sensitive attributes Pale_Skin and Young. Afterwards, we reuse the same hyperparameter values for all tasks with very minor changes (which we verify by running the experiments on the validation set first). The tunable hyperparameters, as well as the range of values that we consider about them, are as follows:

- $\lambda_2 \in \{0, 0.001, 0.0025, 0.005, 0.01, 0.025, 0.05, 0.1, 0.25\}$ – adversarial loss weight;
- $\sigma_{cs} \in \{0.5, 0.55, 0.6, 0.65, 0.7, 0.75\}$ – standard deviation of the Gaussian noise added during center smoothing of R ;
- $\sigma_{rs} \in \{0.1, 0.25, 0.5, 1, 2.5, 5, 10, 25\}$ – standard deviation of the Gaussian noise added during randomized smoothing of C .

Tuning σ_{cs} and the baselines We begin with selecting the value for σ_{cs} . It is not used during the training of R and C , but is an integral part of the center smoothing computation which is performed during inference and is the

most time-consuming component of the model pipeline. More concretely, both $r_{cs} = \hat{R}(\mathbf{z}_G)$ and d_{cs} depend on σ_{cs} , in turn affecting both the accuracy and the certified individual fairness. We evaluate the Naive model with all candidate values for σ_{cs} and show the results in Tab. 9. We observe that there is little variation in terms of accuracy, while the best certified individual fairness and the smallest average center smoothing radii are obtained at $\sigma_{cs} = 0.6$ and 0.65. While there is no significant difference in performance between these two configurations, we expect that the slightly larger value for σ_{cs} would generally produce smaller center smoothing radii, in turn leading to increased certified fairness. Therefore, we set $\sigma_{cs} = 0.65$ for all experiments (except for FairFace, where we use $\epsilon = 0.5$ and scale σ_{cs} correspondingly, i.e., $\sigma_{cs} = 0.325$). Using the same σ_{cs} values for both the baselines and LASSI allows us to attribute the improvements of the results to the additional training mechanisms that we apply and not merely to different hyperparameter values.

We perform a similar evaluation on the validation set of the other baseline, Data Augmentation, and from the results in Tabs. 9 and 10 we set $\sigma_{rs} = 10$ for both Naive and Data Augmentation. Although $\sigma_{rs} = 5$ seems to work slightly better for Young, we remark that Young is also the most fair of all considered sensitive attributes, so we choose a more conservative value that would be suitable for all of them.

Table 10: Results of the Data Augmentation baseline on the validation set of CelebA for $\sigma_{cs} = 0.65$ and different values of σ_{rs} .

Sens. attribute	σ_{cs}	Mean d_{cs}	Metric	σ_{rs}							
				0.1	0.25	0.5	1	2.5	5	10	25
Pale_Skin	0.65	14.52	Acc	87.5	87.5	87.8	87.8	88.7	89.4	88.7	84.9
			Fair	0	0	0	0	0	28.3	31.5	10.0
Young	0.65	7.09	Acc	87.5	87.8	87.8	89.1	88.7	88.7	88.7	84.9
			Fair	0	0	0	1.6	46.6	65.6	65.0	48.9

Tuning λ_2 Next, we incorporate the adversarial loss weight λ_2 to the training and explore its impact on the model in Tab. 11. The certified individual fairness increases with increasing λ_2 , until $\lambda_2 = 0.05$, and stays approximately the same afterwards. Interestingly, the accuracy is mostly unaffected. We set $\lambda_2 = 0.05$ and $\sigma_{rs} = 2.5$ for LASSI, as it gives most of the fairness boost which can be obtained from adversarial training, while keeping the accuracy high. Notably, the hyperparameter tuning demonstrates that LASSI successfully enforces and certifies individual fairness for a wide range of hyperparameter values and is not highly sensitive to them.

Selected experiment hyperparameters Here, we summarize the hyperparameter values selected for the final experiments. We use $\epsilon = 1$ for all similarity set definitions except the experiments with: (i) Denton et al. [57]’s alternative attribute vectors, where $\epsilon = 10$, and (ii) FairFace, where $\epsilon = 0.5$. We maintain the ϵ/σ_{cs} ratio, which impacts the center smoothing [21] results, setting $\sigma_{cs} = 0.65$ by default (as stated in the sections above) and using $\sigma_{cs} = 6.5$ and 0.325 respectively, in the cases when $\epsilon \neq 1$. Consistently with prior work [20, 21], the smoothing arguments we use are as follows:

- Randomized smoothing [20]: $\alpha_{rs} = 0.001$, $N_{rs} = 100,000$, $N_{0,rs} = 2000$.
- Center smoothing [21]: $\alpha_{cs} = 0.01$, $N_{cs} = 10,000$, $N_{0,cs} = 10,000$.

The rest of the model hyperparameters are listed in Tab. 12. In the CelebA 64×64 and 128×128 setups, we run LASSI with $\lambda_2 = 0.25$ for the (target=Earrings, sensitive=Makeup) pair of attributes because of the high correlation between them. We train the representation R for 20 epochs in the transfer experiments (CelebA, FairFace) and 5 epochs otherwise. The linear classifier C is trained for 1 epoch. We generally set a lower value to σ_{rs} when the task is more difficult and the downstream classifier is therefore less confident. When running LASSI on 3D Shapes, we sample more points ($s = 100$) compared to the other datasets in order to accommodate for the more complex similarity sets, defined by many more attribute vectors. Overall, we remark that the hyperparameter values are similar and within the same range for all models and experiments, meaning that our approach does not require substantial fine-tuning.

Table 11: Results of LASSI on the validation subset of CelebA for different values of λ_2 and σ_{rs} , while keeping $\sigma_{cs} = 0.65$. The certified individual fairness increases with increasing λ_2 , until the $\lambda_2 = 0.05$ level.

Sens. attribute	λ_2	Metric	σ_{rs}								
			0.1	0.25	0.5	1	2.5	5	10	25	
Pale_Skin	0.001	Acc	86.5	86.8	87.1	87.5	89.1	89.4	88.1	84.9	
		Fair	0	0	0	0	0	13.2	12.9	1.9	
	0.0025	Acc	87.8	88.1	88.4	88.7	90.4	89.1	86.5	83.3	
		Fair	0	0	0	0	15.4	27.3	24.8	5.5	
	0.005	Acc	87.8	87.8	88.1	87.8	89.7	89.1	87.5	82.0	
		Fair	0	0	0	0	35.0	40.5	37.0	15.4	
	0.01	Acc	88.1	88.1	87.8	88.1	89.4	90.0	87.5	82.0	
		Fair	0	0	0	9.3	46.0	49.5	47.6	27.7	
	0.025	Acc	88.4	88.1	88.1	88.4	89.1	89.7	87.5	82.3	
		Fair	0	1.9	9.6	49.2	64.3	66.2	64.0	47.9	
Young	0.05	Acc	87.8	87.8	88.1	88.1	89.7	89.4	86.8	83.0	
		Fair	45.0	97.1	97.7	98.1	96.1	96.1	95.5	93.6	
	0.1	Acc	86.5	86.5	86.5	86.8	86.5	85.9	83.3	76.8	
		Fair	57.9	93.6	93.9	94.5	96.8	96.1	94.9	88.1	
	0.25	Acc	87.1	87.1	87.1	87.5	87.5	85.9	79.4	67.8	
		Fair	96.8	96.1	96.1	96.1	98.1	97.4	93.2	79.7	
	0.05	Acc	89.1	89.1	88.1	89.4	89.4	89.1	88.7	84.6	
		Fair	97.1	97.7	98.4	99.0	99.0	98.7	96.5	96.1	
	0.1	Acc	88.1	88.7	89.4	89.4	88.7	88.7	87.8	82.6	
		Fair	58.5	94.9	94.9	96.8	97.1	95.8	96.1	92.3	
	0.25	Acc	88.4	88.4	88.4	88.7	88.4	88.1	86.8	77.8	
		Fair	98.4	98.1	98.4	99.4	99.4	98.7	95.2	89.4	

Table 12: Hyperparameter values used for the different model and experiment setups.

Dataset	Model / Experiment(s)	Hyperparameters
CelebA	64×64, 128×128	$\lambda_1 = 1$; $\lambda_2 = 0$ (Naive, DataAug) and 0.05 (LASSI); $\lambda_3 = 0$; $\sigma_{rs} = 10$ (Naive, DataAug) and 2.5 (LASSI); $s = 10$ (DataAug, LASSI).
	Transfer	$\lambda_1 = 0$; $\lambda_2 = 0.05$; $\lambda_3 = 0.1$; $\sigma_{rs} = 0.5$; $s = 10$.
FairFace	Naive	$\lambda_1 = 1$; $\lambda_2 = \lambda_3 = 0$; $\sigma_{rs} = 5$ (Age-2) and 0.1 (Age-3, Age (all)).
	LASSI	$\lambda_1 = 1$; $\lambda_2 = 0.1$; $\lambda_3 = 0$; $\sigma_{rs} = 0.25$; $s = 10$.
	Transfer	$\lambda_1 \in \{0, 0.001, 0.01\}$; $\lambda_2 = \lambda_3 = 0.1$; $\sigma_{rs} = 0.1$; $s = 10$.
3D Shapes	Naive	$\lambda_1 = 1$; $\lambda_2 = \lambda_3 = 0$; $\sigma_{rs} = 5$ (orientation) and 2.5 (scale).
	LASSI	$\lambda_1 = 1$; $\lambda_2 = 0.1$; $\lambda_3 = 0$; $\sigma_{rs} = 1$; $s = 100$.

D More Experimental Results on CelebA

In this section we provide further details about the experiments on the CelebA dataset.

64×64 images Tab. 13 and 14 contain the means and the standard deviations of the accuracies and the certified individual fairness respectively of the CelebA 64×64 experiments summarized in Tab. 1, averaged over 5 runs. The standard deviation of Naive and DataAug’s fairness is high, while LASSI consistently enforces certified individual fairness with low variance.

Table 13: Means and standard deviations of the accuracies reported in Tab. 1, averaged over 5 runs with different random seeds.

Task	Sensitive attribute(s)	Naive	DataAug [61]	LASSI (ours)
Smiling	Pale_Skin	86.3 ± 1.5	85.7 ± 1.2	85.9 ± 1.3
	Young	86.3 ± 1.8	85.9 ± 1.6	86.3 ± 1.3
	Blond_Hair	86.3 ± 1.6	86.6 ± 1.0	86.4 ± 1.0
	Heavy_Makeup	86.3 ± 1.1	85.3 ± 1.7	85.6 ± 1.6
	Pale+Young	86.0 ± 1.5	85.8 ± 1.4	85.8 ± 0.9
	Pale+Young+Blond	86.2 ± 1.7	86.4 ± 1.0	85.5 ± 0.4
Earrings	Pale_Skin	81.33 ± 2.2	81.0 ± 2.3	85.0 ± 0.5
	Young	81.4 ± 2.2	79.9 ± 1.4	84.5 ± 1.0
	Blond_Hair	81.4 ± 2.2	82.2 ± 2.8	84.8 ± 0.5
	Heavy_Makeup	81.6 ± 1.9	80.3 ± 1.9	82.3 ± 0.6

Table 14: Means and standard deviations of the certified individual fairness reported in Tab. 1, averaged over 5 runs.

Task	Sensitive attribute(s)	Naive	DataAug [61]	LASSI (ours)
Smiling	Pale_Skin	0.6 ± 0.5	12.2 ± 14.7	98.0 ± 0.5
	Young	38.2 ± 23.4	43.0 ± 30.7	98.8 ± 0.6
	Blond_Hair	3.4 ± 3.1	9.4 ± 10.0	94.7 ± 1.5
	Heavy_Makeup	0.4 ± 0.4	13.7 ± 8.8	91.3 ± 8.1
	Pale+Young	0.4 ± 0.4	9.9 ± 12.7	97.3 ± 0.9
	Pale+Young+Blond	0.0 ± 0.0	3.6 ± 3.8	86.5 ± 2.7
Earrings	Pale_Skin	24.3 ± 35.6	40.4 ± 32.6	98.5 ± 0.9
	Young	59.2 ± 18.0	72.0 ± 24.1	98.0 ± 1.1
	Blond_Hair	9.2 ± 17.5	30.5 ± 40.9	96.2 ± 2.6
	Heavy_Makeup	20.5 ± 13.0	49.2 ± 37.0	98.7 ± 0.7

Moreover, in Tab. 15 we check for what fraction of the test subset the models classify the endpoints of the similarity sets the same as the original data point. Note that this is again another empirical estimate, serving as an upper bound of the certified individual fairness of the models. Nevertheless, LASSI outperforms the baselines on that metric as well. More importantly, out of all 150 combinations of models, tasks and sensitive attributes (3 model types, 10 task-attribute pairs, 5 random seeds) in only 8 of them there is just 1 test sample which we certify as individually fair but the endpoints classifications of the models mismatch. For all other combinations no such situation occurs, serving as another test for the correctness of our certificates. One test sample out of 312 is 0.32%, which is within our confidence of $1 - \alpha_{cs} - \alpha_{rs} = 98.9\%$.

Table 15: Empirical evaluation of the individual fairness of the models computed by comparing their predictions on the original test samples to the model predictions on the endpoints of the corresponding similarity sets.

Task	Sensitive attribute(s)	Naive	DataAug [61]	LASSI (ours)
Smiling	Pale_Skin	78.4 ± 2.1	90.1 ± 1.9	99.6 ± 0.2
	Young	95.3 ± 0.4	96.7 ± 0.5	99.6 ± 0.2
	Blond_Hair	83.3 ± 0.7	93.9 ± 1.5	99.2 ± 0.4
	Heavy_Makeup	75.8 ± 2.4	88.3 ± 0.8	97.9 ± 1.6
	Pale+Young	78.0 ± 2.0	89.0 ± 2.2	99.4 ± 0.5
	Pale+Young+Blond	77.9 ± 2.1	87.4 ± 0.9	96.9 ± 0.7
Earrings	Pale_Skin	97.1 ± 1.6	99.1 ± 0.7	99.5 ± 0.4
	Young	98.5 ± 1.4	99.5 ± 0.5	99.2 ± 0.4
	Blond_Hair	96.7 ± 3.4	98.5 ± 0.4	99.1 ± 0.7
	Heavy_Makeup	92.2 ± 6.6	98.1 ± 1.1	99.7 ± 0.3

128×128 images Tab. 16 and 17 contain the results for 128×128-dimensional images.

Different attribute vectors The means and standard deviations of the accuracies and the certified individual fairness from Tab. 2 are reported in Tab. 18 and 19 respectively.

Table 16: Means and standard deviations of the accuracies on 128×128 images.

Task	Sensitive attribute(s)	Naive	DataAug [61]	LASSI (ours)
Smiling	Pale_Skin	88.8 ± 1.0	89.6 ± 0.5	90.0 ± 1.1
	Young	88.7 ± 0.7	88.8 ± 1.0	89.7 ± 0.7
	Blond_Hair	88.8 ± 0.9	89.4 ± 1.1	90.1 ± 0.8
	Heavy_Makeup	89.0 ± 0.9	89.6 ± 1.1	90.2 ± 0.3
	Pale+Young	88.8 ± 1.0	89.4 ± 1.3	90.2 ± 0.5
	Pale+Young+Blond	88.7 ± 0.8	89.9 ± 1.5	90.2 ± 0.7
Earrings	Pale_Skin	80.1 ± 1.4	80.1 ± 2.5	84.4 ± 0.9
	Young	80.2 ± 1.4	80.3 ± 1.5	85.5 ± 1.4
	Blond_Hair	80.2 ± 1.4	80.6 ± 2.0	83.9 ± 0.9
	Heavy_Makeup	80.3 ± 1.4	80.1 ± 1.9	81.7 ± 1.3

Table 17: Means and standard deviations of the certified individual fairness on 128×128 images.

Task	Sensitive attribute(s)	Naive	DataAug [61]	LASSI (ours)
Smiling	Pale_Skin	0.0 ± 0.0	0.0 ± 0.0	70.6 ± 14.2
	Young	46.0 ± 16.2	47.6 ± 20.2	97.2 ± 1.6
	Blond_Hair	0.1 ± 0.1	0.0 ± 0.0	77.8 ± 10.2
	Heavy_Makeup	2.5 ± 3.5	30.4 ± 20.7	87.6 ± 3.9
	Pale+Young	0.0 ± 0.0	8.7 ± 16.5	69.4 ± 9.7
	Pale+Young+Blond	0.0 ± 0.0	4.4 ± 9.6	72.7 ± 5.0
Earrings	Pale_Skin	0.0 ± 0.0	0.1 ± 0.1	90.4 ± 2.5
	Young	73.5 ± 20.4	78.2 ± 18.1	96.4 ± 1.7
	Blond_Hair	0.0 ± 0.0	0.0 ± 0.0	89.7 ± 4.0
	Heavy_Makeup	42.1 ± 15.9	65.1 ± 31.1	98.3 ± 1.3

Table 18: Means and standard deviations of the accuracies from Tab. 2.

Task	Sensitive attribute(s)	Naive	DataAug [61]	LASSI (ours)
Smiling	Pale_Skin	86.4 ± 1.7	85.9 ± 1.5	86.5 ± 1.3
	Young	86.3 ± 1.8	86.2 ± 1.5	86.8 ± 1.0
	Blond_Hair	86.2 ± 1.8	86.1 ± 1.8	86.7 ± 1.4
	Heavy_Makeup	86.2 ± 1.6	86.3 ± 1.1	86.8 ± 1.0
	Pale+Young	86.2 ± 1.8	85.8 ± 1.5	86.5 ± 1.2
	Pale+Young+Blond	86.2 ± 1.7	85.9 ± 1.8	86.4 ± 1.1

Table 19: Means and standard deviations of the certified individual fairness from Tab. 2.

Task	Sensitive attribute(s)	Naive	DataAug [61]	LASSI (ours)
Smiling	Pale_Skin	34.0 ± 5.4	90.3 ± 3.9	98.8 ± 1.2
	Young	73.1 ± 3.5	90.3 ± 3.3	97.9 ± 1.2
	Blond_Hair	71.4 ± 4.0	88.8 ± 2.7	98.8 ± 0.7
	Heavy_Makeup	11.5 ± 2.5	87.4 ± 1.6	98.8 ± 0.9
	Pale+Young	28.6 ± 3.4	84.7 ± 4.1	98.6 ± 1.8
	Pale+Young+Blond	23.7 ± 2.1	82.2 ± 5.2	98.7 ± 0.5

Transfer learning Tab. 20 has the base standard accuracies of the transfer tasks. Tab. 21 reports the means and the standard deviations of LASSI on the Smiling task when solved in a transfer learning setting.

Table 20: Baseline accuracies for the transfer CelebA tasks. As before, the ResNet-18 classifier takes the original images as an input, while the z_G classifier is a fully connected network classifying their Glow latent representations. Neither of these classifiers involves representation learning.

Task	Majority class		Acc (ResNet-18)		Acc (z_G)	
	Valid	Test	Valid	Test	Valid	Test
Smiling	51.7	52.6	92.1 ± 0.2	90.9 ± 0.7	89.4 ± 0.1	87.2 ± 1.1
High_Cheeks	55.1	51.9	87.2 ± 0.2	86.8 ± 0.4	84.3 ± 0.1	83.8 ± 0.7
Mouth_Open	51.8	53.8	92.7 ± 0.3	92.9 ± 0.7	88.1 ± 0.2	89.6 ± 1.1
Lipstick	55.4	54.8	91.5 ± 0.2	90.5 ± 0.8	89.2 ± 0.1	90.6 ± 1.1
Heavy_Makeup	61.0	58.7	90.2 ± 0.4	89.9 ± 0.4	87.8 ± 0.1	88.6 ± 1.1
Wavy_Hair	72.3	65.1	82.7 ± 1.8	76.3 ± 3.3	80.9 ± 0.5	81.7 ± 0.4
Eyebrows	74.2	71.8	83.5 ± 0.5	81.1 ± 0.6	80.1 ± 0.1	79.4 ± 1.6

Table 21: Mean and standard deviation of the accuracy and the certified individual fairness of LASSI on the Smiling task solved in a transfer learning setting (Tab. 3).

Task	Sensitive attribute(s)	Acc	Fair
Smiling	Pale_Skin	86.2 ± 1.1	93.1 ± 2.4
	Young	86.0 ± 1.2	95.4 ± 1.0
	Blond_Hair	85.1 ± 1.6	93.8 ± 1.8
	Pale+Young	85.9 ± 0.3	92.2 ± 0.7
	Pale+Young+Blond	85.1 ± 0.7	87.0 ± 2.3

E More Examples of Similar Individuals

Here, we provide further examples of points from the similarity sets $S_i(\mathbf{x})$, as reconstructed by Glow, for various inputs \mathbf{x} randomly drawn from the test sets which we consider in our evaluation. A summary of all configurations is listed in Tab. 22. The images in the middle of the CelebA and FairFace reconstructions correspond to the original inputs. The perturbations range uniformly in the $[-\frac{\epsilon}{\sqrt{n}}, \frac{\epsilon}{\sqrt{n}}]$ interval, where n is the number of sensitive attributes. For $n > 1$, all attribute vectors are multiplied by the same t before they are added to the latent representation of the original inputs. We set $\epsilon = 1$ for CelebA and 3D Shapes and $\epsilon = 0.5$ for FairFace.

Table 22: Summary of the provided example images from the similarity sets considered in this work.

Dataset	Sensitive attribute(s)	Figure
CelebA	Pale_Skin	Fig. 6
	Young	Fig. 7
	Blond_Hair	Fig. 8
	Heavy_Makeup	Fig. 9
	Pale + Young	Fig. 10
FairFace	Pale + Young + Blond	Fig. 11
	Race=Black	Fig. 12
3D Shapes	orientation	Fig. 13

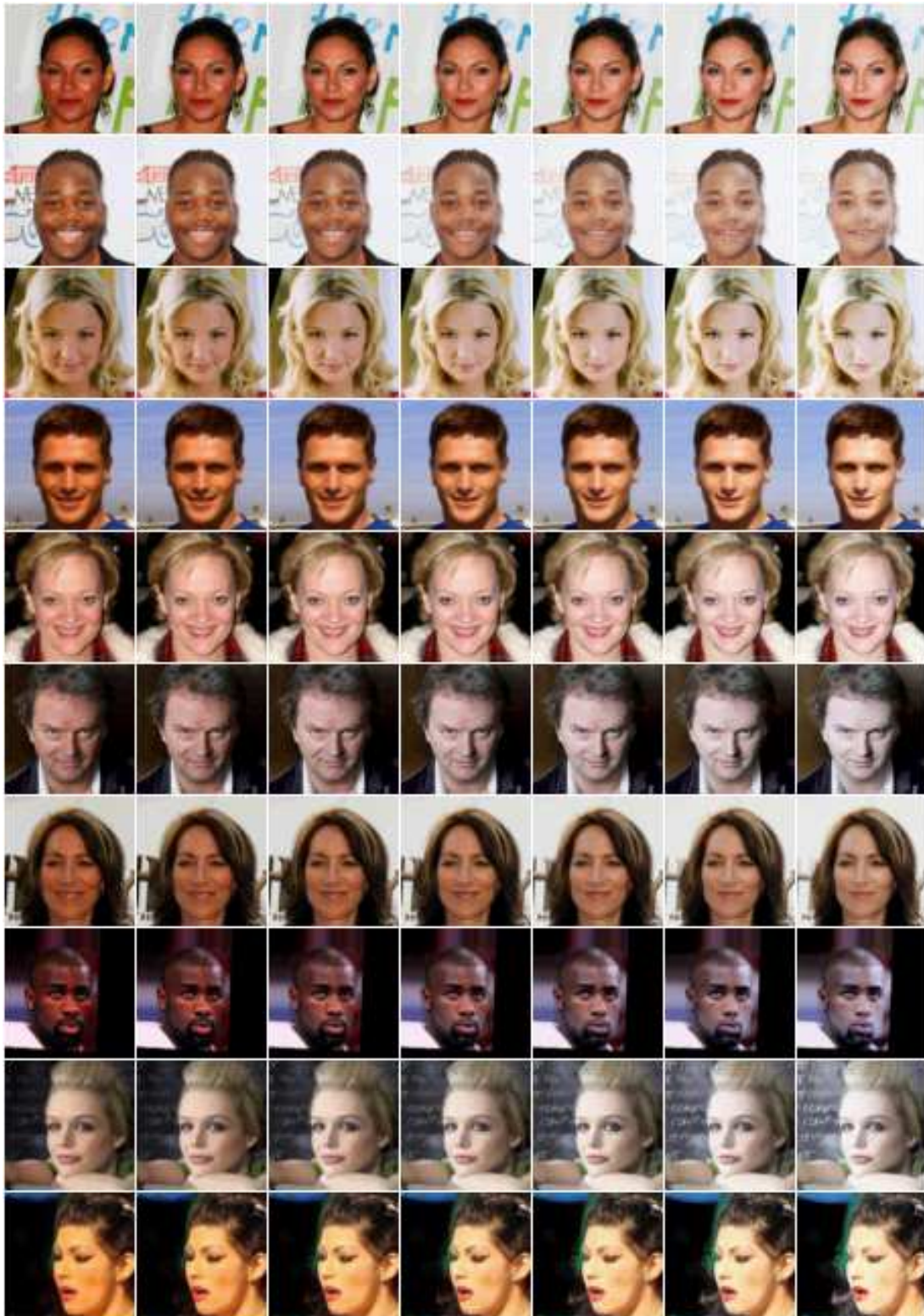


Figure 6: Similar individuals from $S_i(x)$, for x in the CelebA dataset, obtained by varying the sensitive attribute `Pale_Skin`.

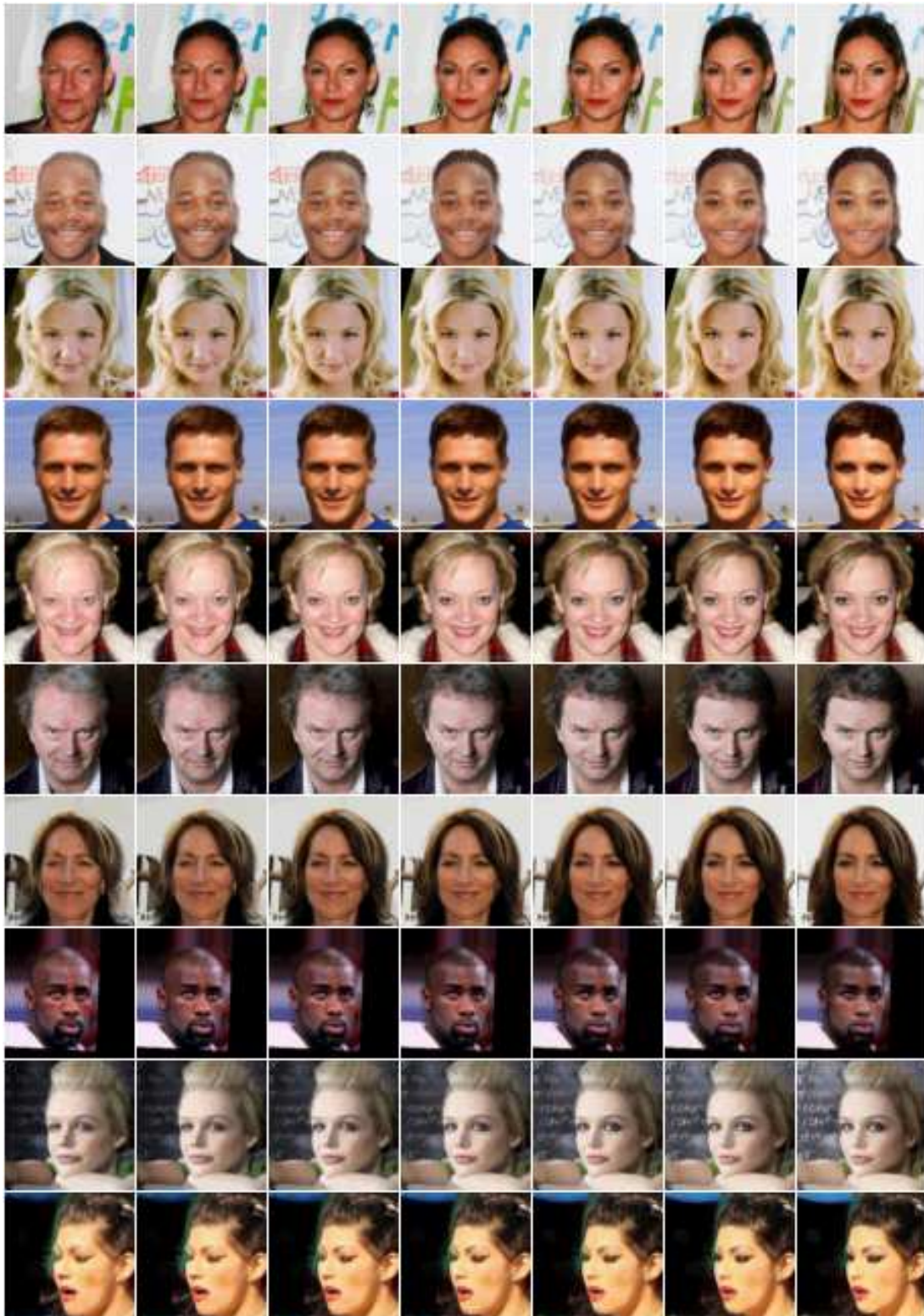


Figure 7: Similar individuals from $S_i(x)$, for x in the CelebA dataset, obtained by varying the sensitive attribute Young.



Figure 8: Similar individuals from $S_i(x)$, for x in the CelebA dataset, obtained by varying the sensitive attribute `Blond_Hair`.

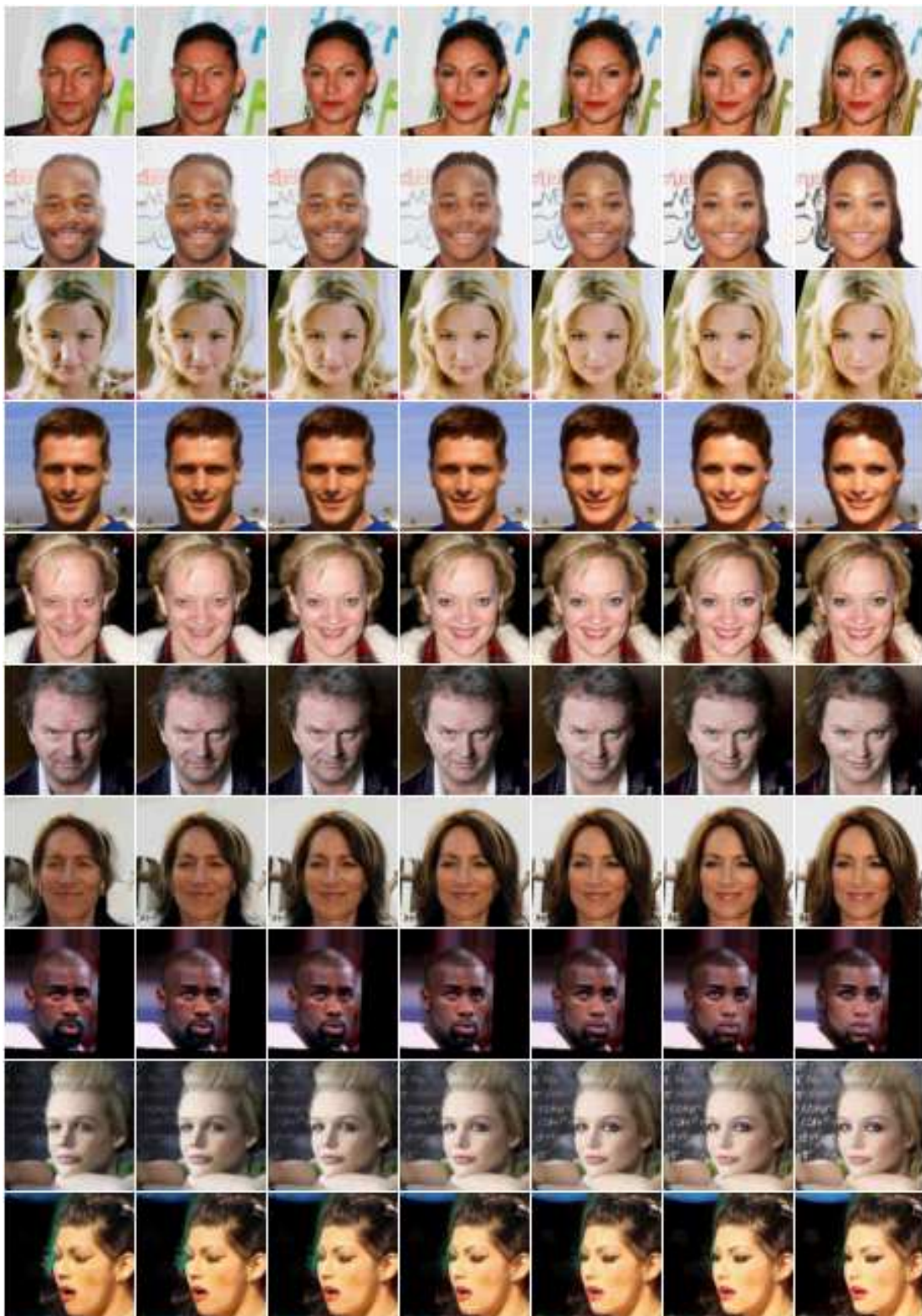


Figure 9: Similar individuals from $S_i(x)$, for x in the CelebA dataset, obtained by varying the sensitive attribute Heavy_Makeup.

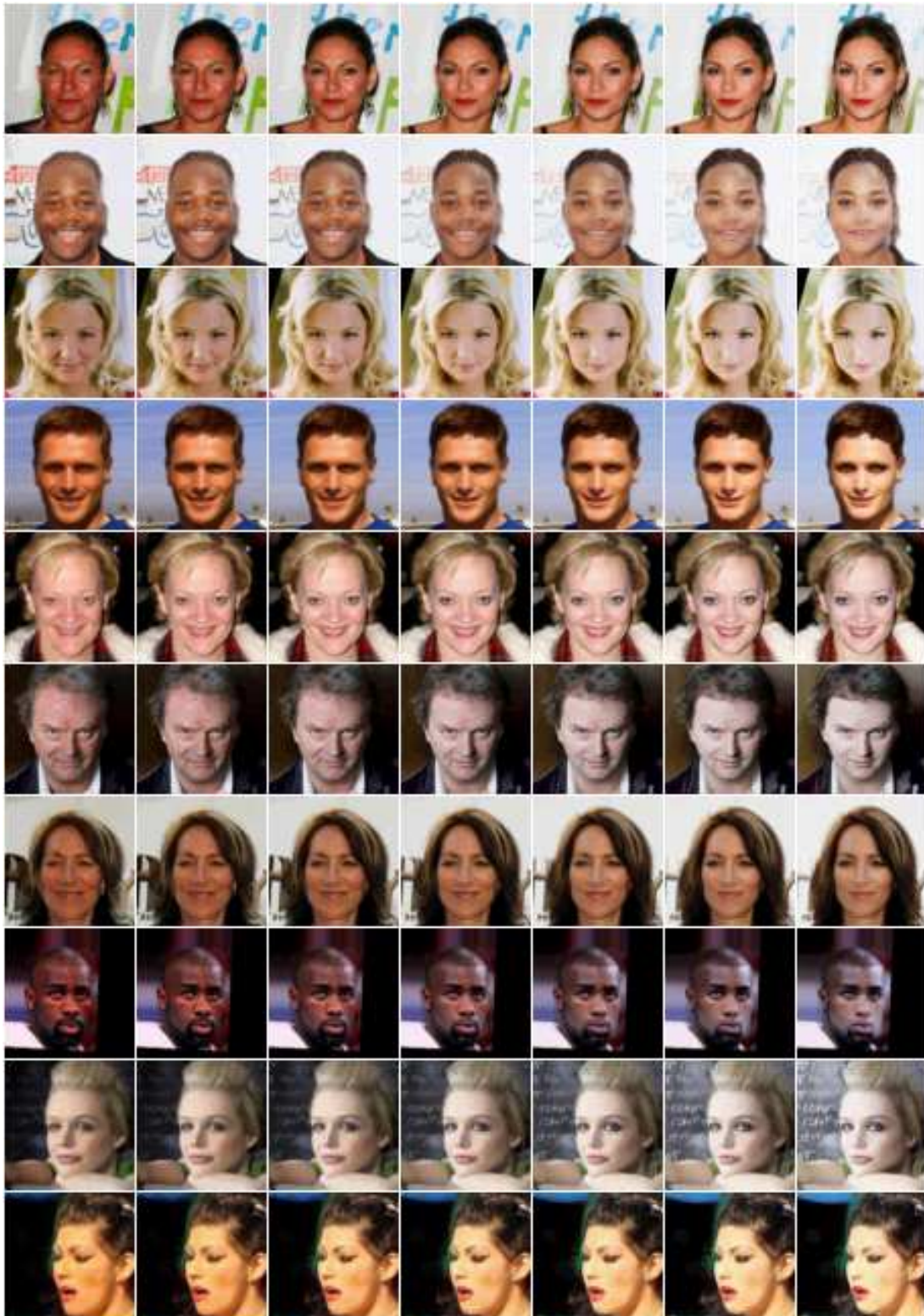


Figure 10: Similar individuals from $S_i(\mathbf{x})$ obtained by simultaneously varying the sensitive attributes Pale_Skin + Young.

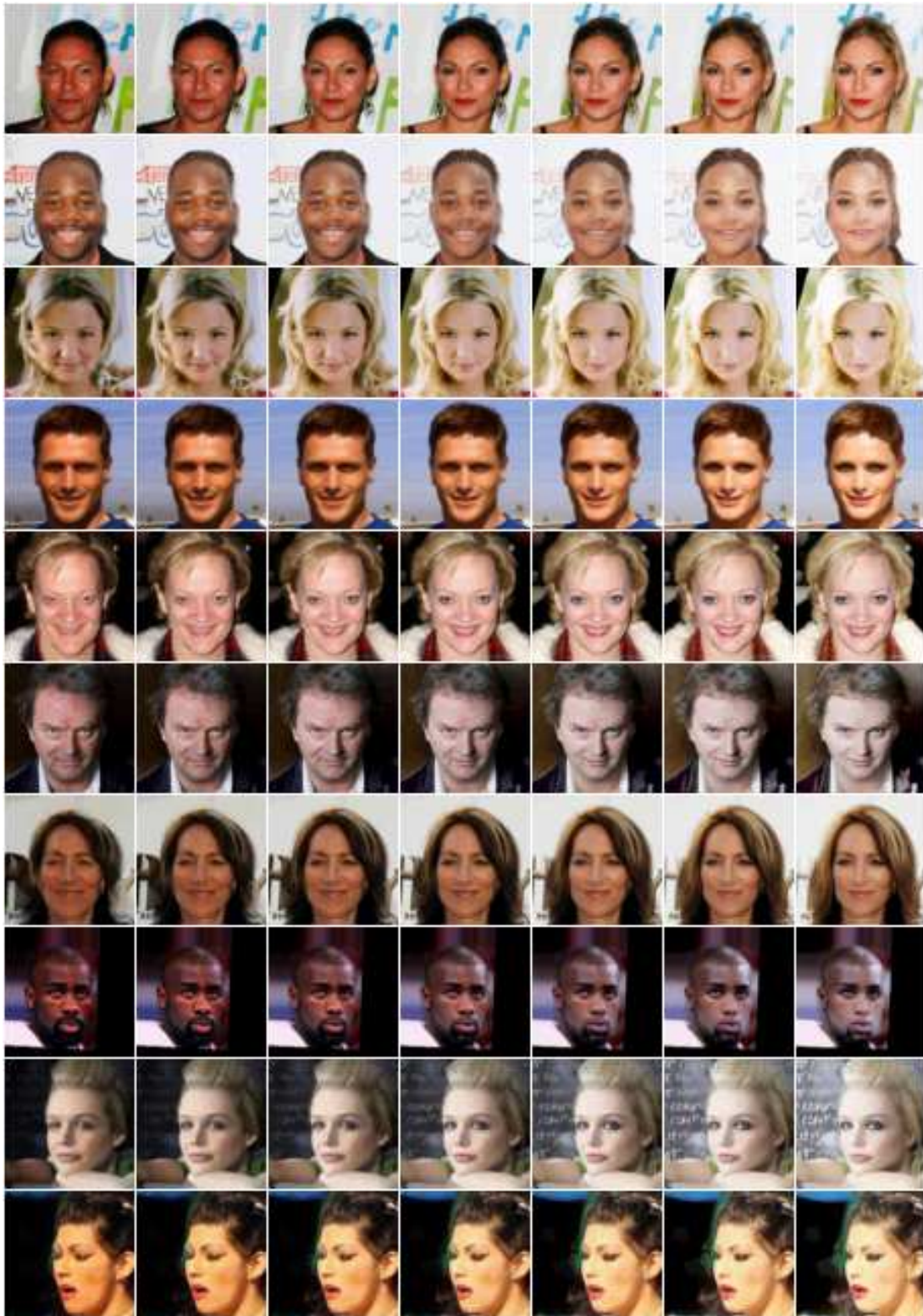


Figure 11: Similar individuals from $S_i(\mathbf{x})$ obtained by simultaneously varying the sensitive attributes Pale_Skin + Young + Blond.

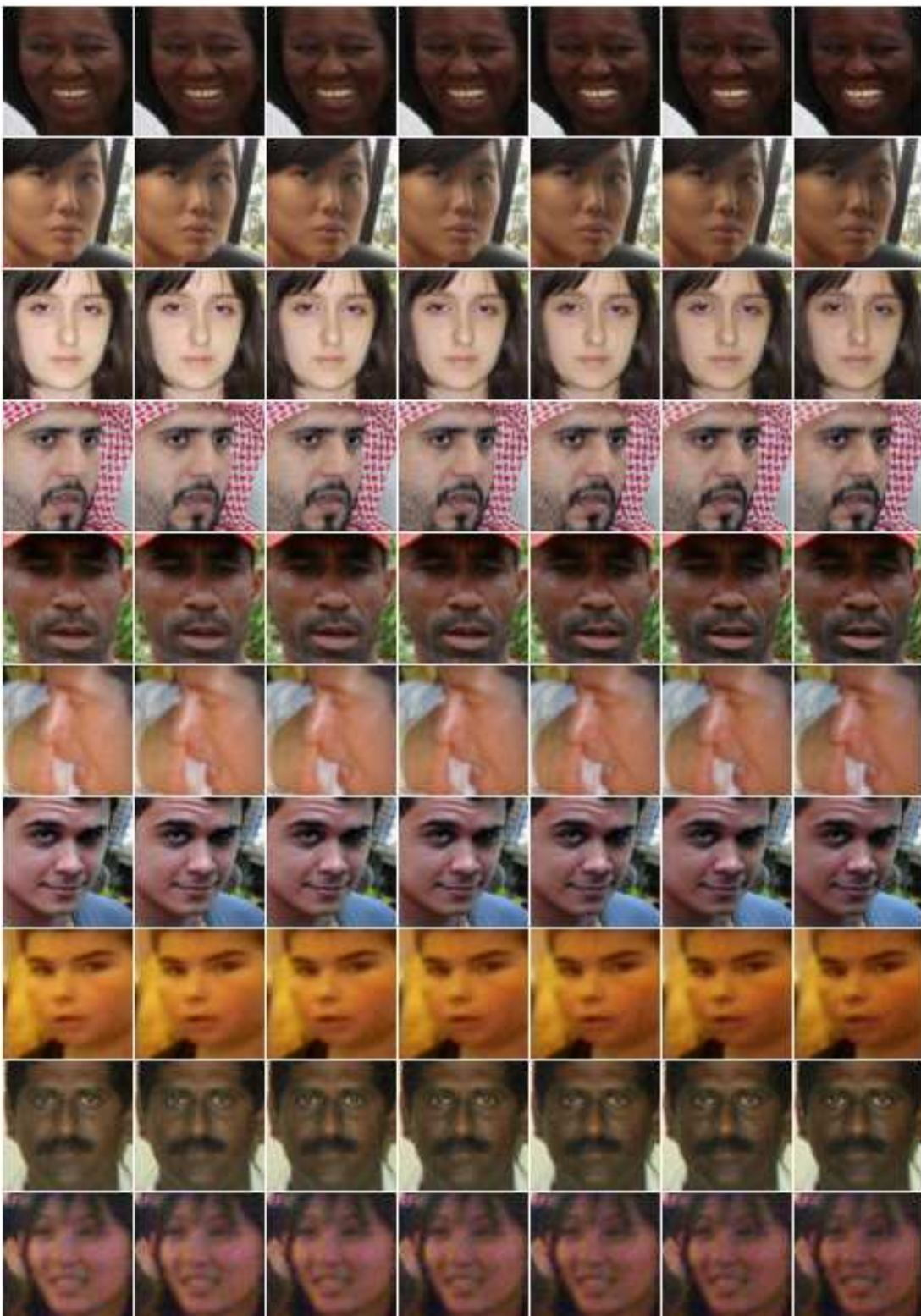


Figure 12: Similar individuals from $S_i(x)$, for x in FairFace and $\epsilon = 0.5$, obtained by varying the sensitive attribute Race=Black.

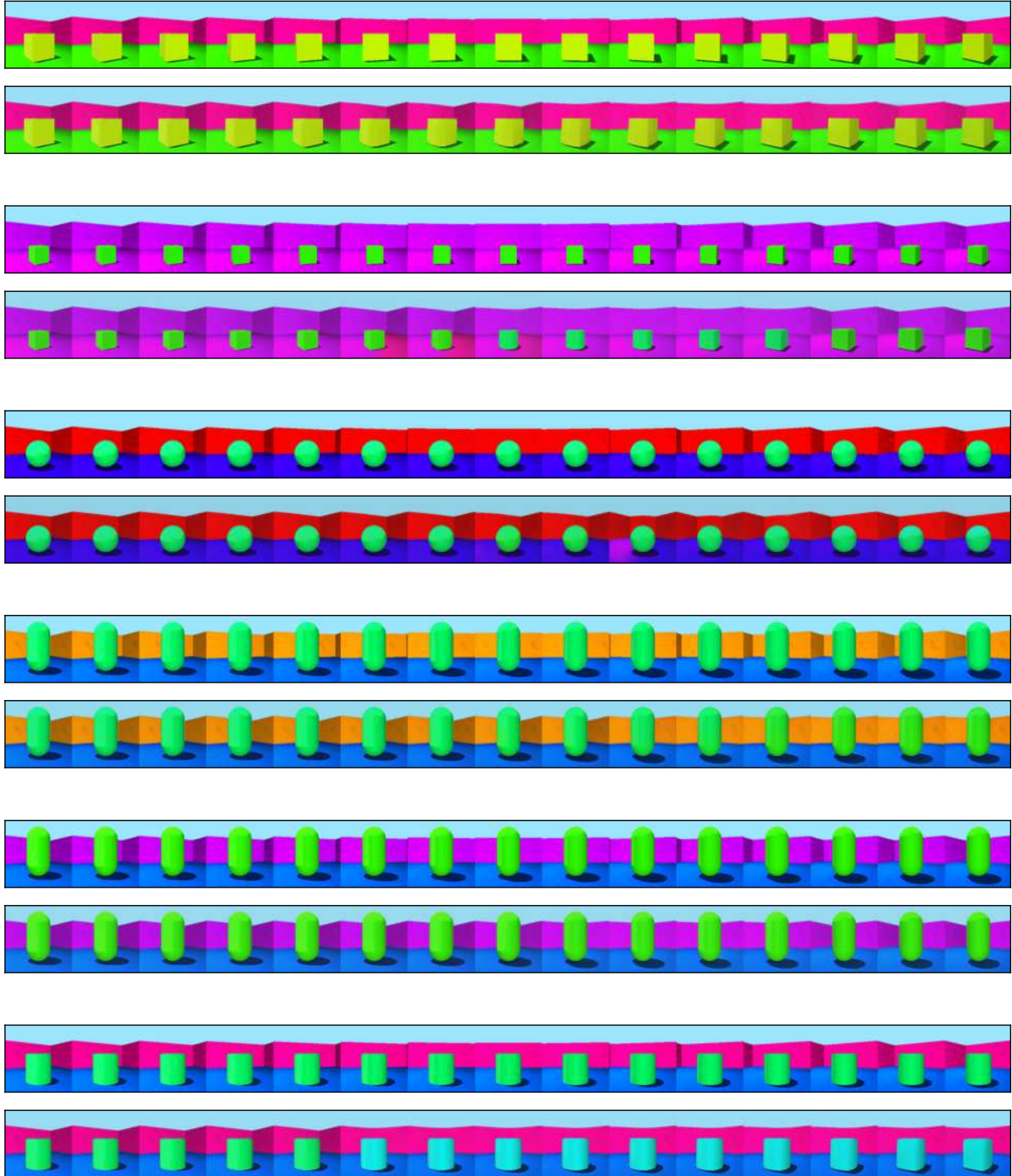


Figure 13: Sampled shapes at 15 different ground truth orientations. The original (above) and the corresponding reconstructions (below) obtained from interpolating along one of the generative model's attribute vectors, $\alpha_{1,15}$, grouped together.